AWARD NUMBER: W81XWH-13-1-0240

TITLE: Targeted, On-Demand Charge Conversional Nanotherapeutics for Advanced Prostate Cancer

PRINCIPAL INVESTIGATOR: Xuli Wang, Ph.D.

CONTRACTING ORGANIZATION: University of Utah
Salt Lake City, UT 84112

REPORT DATE: September 2016

TYPE OF REPORT: Annual

PREPARED FOR: U.S. Army Medical Research and Materiel Command
Fort Detrick, Maryland 21702-5012

REPORT DOCUMENTATION PAGE

Form Approved
OMB No. 0704-0188

1. REPORT DATE	2. REPORT TYPE	3. DATES COVERED
September 2016	Annual	29 Aug 2015 – 28 Aug 2016

4. TITLE AND SUBTITLE
Targeted, On-Demand Charge Conversional Nanotherapeutics for Advanced Prostate Cancer

5a. CONTRACT NUMBER

5b. GRANT NUMBER
W81XWH-13-1-0240

5c. PROGRAM ELEMENT NUMBER

6. AUTHOR(S)

Xuli Wang, Ph.D.
E-Mail: xuli.wang@utah.edu

5d. PROJECT NUMBER

5e. TASK NUMBER

5f. WORK UNIT NUMBER

7. PERFORMING ORGANIZATION NAME(S) AND ADDRESS(ES)
University of Utah
Salt Lake City, UT, 84112

8. PERFORMING ORGANIZATION REPORT NUMBER

9. SPONSORING / MONITORING AGENCY NAME(S) AND ADDRESS(ES)

U.S. Army Medical Research and Materiel Command
Fort Detrick, Maryland 21702-5012

10. SPONSOR/MONITOR'S ACRONYM(S)

11. SPONSOR/MONITOR'S REPORT NUMBER(S)

12. DISTRIBUTION / AVAILABILITY STATEMENT

Approved for Public Release; Distribution Unlimited

13. SUPPLEMENTARY NOTES

14. ABSTRACT

In this project, we have proposed to design and test an innovative nanotherapeutic system to attack prostate cancer occurred in skeletal tissue. The proposed targeted, bio-responsive nanotherapeutics are based on peptide-functionalized diblock copolymers of poly(ethylene glycol) and poly(trimethenecarbonate) (PEG-PTMC) as the drug carrier, by using docetaxel as the therapeutic agent. During the past funding period, copolymers with predetermined terminal functionality, molecular weights and chemical compositions have been synthesized, and the physicochemical properties of nanotherapeutics including drug loading capacity and drug release profile have been investigated. The peptide functionalized nanotherapeutics possess high HA binding affinity, indicating their good bone-targeting capacity. We have investigated and evaluated biological activities of the drug-loaded nanotherapeutics in terms of cellular uptake and tumor inhibition in cultured prostate cancer cells. We have also initiated bone uptake and retention of the proposed nanotherapeutics in mice. For the future study, we will further perform therapeutic efficacy studies in vivo, such as survival study and bone-related therapeutic evaluation of bone-targeted nanotherapeutics to improve therapy for advanced prostate cancers.

15. SUBJECT TERMS
Prostate cancer, bone metastasis, bone-targeting, drug delivery system

16. SECURITY CLASSIFICATION OF:			17. LIMITATION OF ABSTRACT	18. NUMBER OF PAGES	19a. NAME OF RESPONSIBLE PERSON
a. REPORT	b. ABSTRACT	c. THIS PAGE			19b. TELEPHONE NUMBER *(include area code)*
U	U	U	UU	36	USAMRMC

Standard Form 298 (Rev. 8-98)
Prescribed by ANSI Std. Z39.18

Table of Contents

Page

1. **INTRODUCTION:**

Advanced prostate cancer frequently leads to skeletal complications that are very difficult to treat and result in pain, bone fractures, nerve compression, morbidity, and often mortality, and it is considered to be an incurable disease. Current therapeutic options are usually palliative in nature and there is a clear need for better treatment options for bone metastatic prostate cancers. This proposal addresses such an important public health need. Specifically, this project proposes a novel osteotropic, bio-responsive, and prostate-specific drug delivery system for advanced prostate cancer induced bone metastases. The proposed nanotherapeutic system using a multilevel targeting strategy could lead to a more effective approach to attack prostate cancers. The nanotherapeutics possess favorable pharmacological features to improve bioavailability. Additionally, such a therapeutic strategy to deliver therapeutic agents into metastatic bone microenvironments may lead to a potential synergistic effect and improve overall therapeutic efficacy.

2. **KEYWORDS:** Prostate cancer, bone metastasis, bone-targeting, drug delivery system

3. **ACCOMPLISHMENTS:**

What were the major goals of the project?

In this application, we have proposed to design and test an innovative nanotherapeutic system to attack prostate cancer occurred in skeletal tissue. The proposed targeted, bio-responsive nanotherapeutics are based on a peptide functionalized diblock copolymers of poly(ethylene glycol) and poly(trimethenecarbonate) (PEG-PTMC) as the drug carrier, by using docetaxel as the therapeutic agent. Copolymers with predetermined terminal functionality, molecular weights and chemical compositions were synthesized to fine-tune the amphiphilicity, solubility and drug loading capacity of the carriers. We have evaluated the physicochemical properties of nanotherapeutics including size, drug loading capacity, and drug release profile. We have performed studies to determine *in vivo* HA binding affinity, *in vivo* bone uptake and retention of the nanotherapeutics. The nanotherapeutics have been extensively investigated in cultured prostate cells to determine biological properties in terms of CTSK-triggered cellular uptake and anti-tumor efficacy. Finally, animals with prostate cancer induced bone metastases were established in order to test the proposed nanotherapeutics *in vivo*.

What was accomplished under these goals?

To accomplish the objectives of the proposed research, the following tasks have been achieved:

Task 1: Synthesize and characterize the nanotherapeutic constructs.

Task 2: Determine *in vitro* HA binding affinity, *in vivo* bone uptake and retention of the Asp8-containing nanoparticles.

Task 3: Investigate and evaluate biological activities of the docetaxel-loaded nanotherapeutics in terms of cellular uptake and tumor inhibition in cultured prostate cancer cells.

Task 4: Therapeutic evaluation of the proposed nanotherapeutics and appropriate controls in mice with prostate cancer induced bone metastases.

During the first year of the research project, we have completed the synthesis and characterization of block copolymer based drug carriers for bone-targeted, bio-responsive nanotherapeutics for advanced prostate cancer therapy, and the drug-loaded nanoparticles (i.e. nanotherapeutics) were achieved by conjugation of functional moiety (CK(DUPA)GHPGGPQAsp8) with a bone tropism domain, a CTSK-cleavable substrate, and a prostate-specific ligand. A variety of experiments have been performed to investigate and evaluate biological activities of the nanotherapeutics in terms of cellular uptake and tumor inhibition in cultured prostate cancer cells by using dynamic light scattering (DLS), confocal laser scanning microscopy (CLSM), fluorescence-activated cell sorting (FACS), and MTT cell proliferation assay. In addition, we have confirmed that Asp8-containing nanoparticles are favorable for bone uptake and retention in comparison with Asp8-free nanoparticles in vivo. Some results have been summarized as below.

For chemical synthesis, copolymers with terminus of maleimide functional group as well as their respective control copolymers with non-functional methyloxyl group, have been obtained via ring-opening polymerization synthetic strategy. The synthetic procedure and reaction condition for preparation of methoxyl- (Scheme 1 (a)) or maleimide- (Scheme 1 (b)) terminated polymers were illustrated in the Figure 1. Typical ^{1}H NMR spectra for block copolymers with maleimide-terminus or methyloxyl-terminus have been shown in Figure 1.

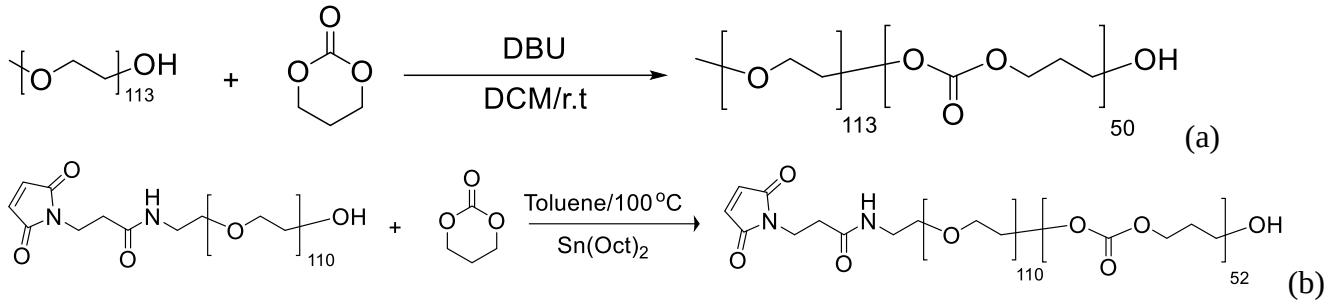

Scheme 1: Synthesis of copolymers with terminus of methoxyl- (a) or maleimide functional group (b)

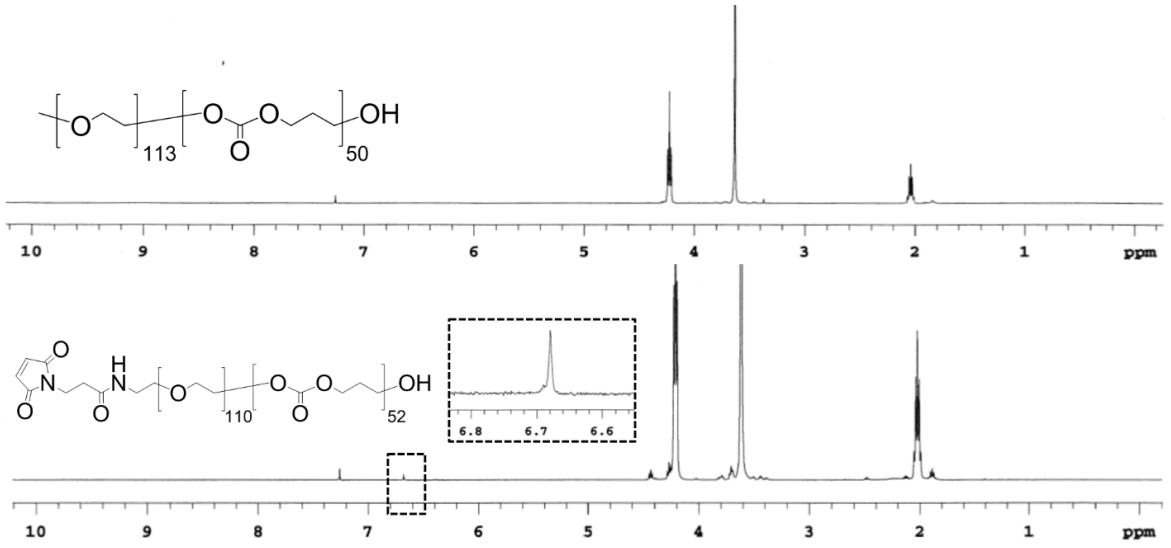

Figure 1. ^{1}H NMR spectra of block copolymer PEG-PTMC without (upper panel) and with (lower panel) maleimide functional group.

Furthermore, based on Solid-Phase Peptide Synthesis (SPPS) strategy, a functional peptide with sequence of CKGHPGGPQAsp8 has been successfully obtained. Briefly, the functional peptide was synthesized by using Rink amide resin solid support and HBTU/HOBt as coupling reagents. Coupling efficiencies were monitored by the Kaiser ninhydrin test. The peptide was cleaved from the resin by treatment with TFA/EDT/H_2O/TIBS (94/2.5/2.5/1) mixture as scavengers. The crude was precipitated with cold ethyl ether and purified by preparative RP-HLPC. The purity of peptide was checked by analytical RP-HPLC. Typical HPLC profile for the peptide has been shown in Figure 2. Its molecular weight was confirmed by mass spectroscopy, as shown in Figure 3.

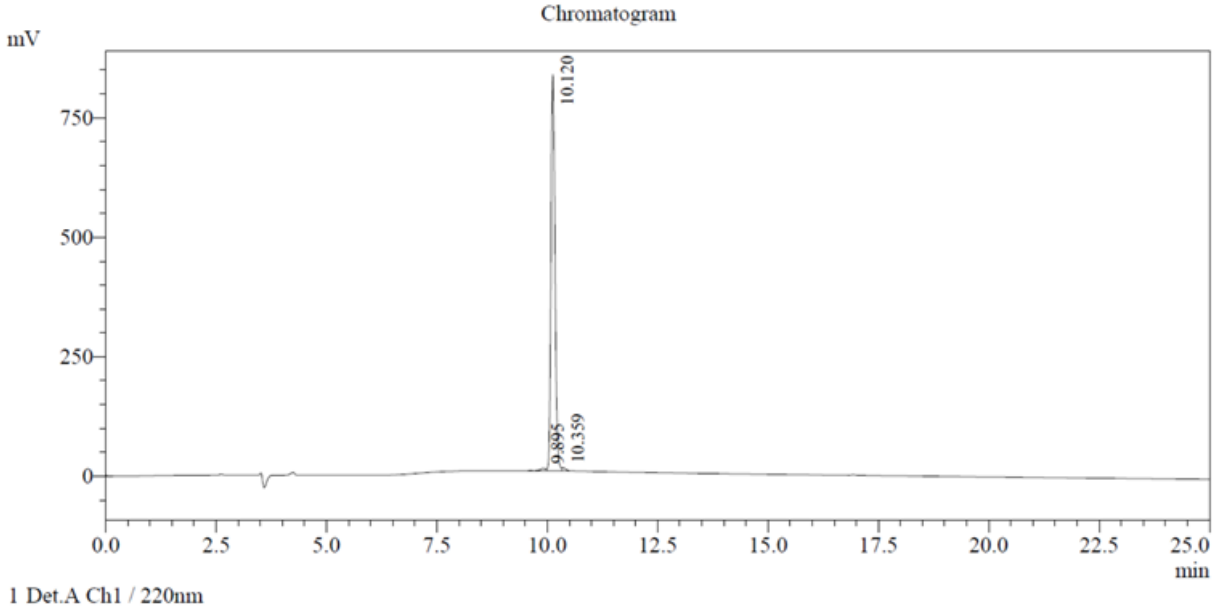

Figure 2. HPLC profile of CKGHPGGPQAsp$_8$ demonstrates its high purity (>98%)

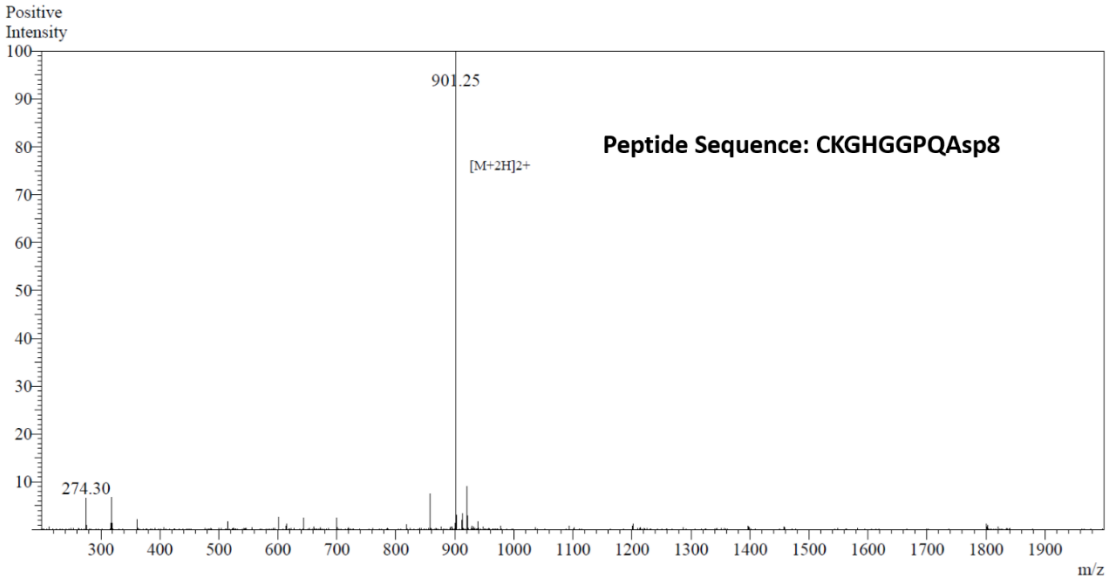

Figure 3. Molecular weight characterization of peptide (CKGHGGPQAsp$_8$).

Ligand DUPA was synthesized according to Scheme 2. Briefly, to a dried three-neck flask was added L-glutamate di-tert-butyl ester hydrochloride (1.2 g) and 100 mL of DCM under nitrogen atmosphere. After the solution was cooled to -65 ^oC, triphosgene (400 mg) and 1.25

mL of triethylamine were added. Then this solution was stirred for 6 h and temperature gradually raised from -65 ^{o}C to 4 ^{o}C under the protection of nitrogen. The solution was re-cooled to -65 ^{o}C before adding a solution of L-Glu(OBn)-OtBu (1.5 g) and triethylamine (1.5 mL) in DCM (50 mL). The reaction mixture was allowed to increase to room temperature over a period of 2 h and stirred at room temperature overnight. The reaction was quenched with HCl, and the organic layer was washed with water, brine and dried over anhydrous sodium sulfate. The crude product was purified using flash chromatography to obtain product as colorless oil. This compound (1 g, 1.73 mmol) was dissolved in 30 mL of DCM, then 10% Pd/C (200 mg) was added into this solution. The reaction mixture was hydrogenated at 1 atm for 24 h at room temperature. Pd/C was filtered through a Celite pad and washed with DCM. The crude product was purified by using flash chromatography to obtain the desired product as white solid.

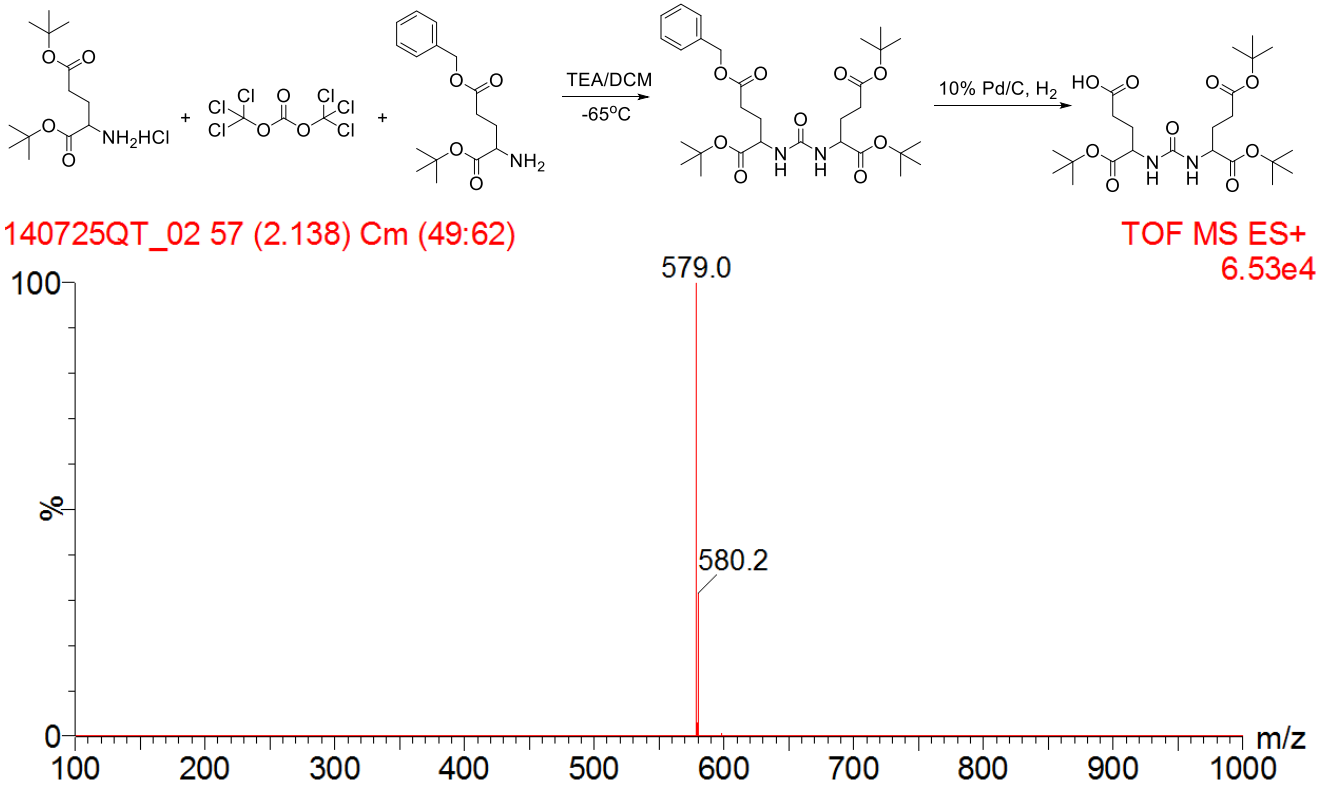

Figure 4: Synthesis and molecular weight characterization of DUPA ligand

Conjugation DUPA onto peptide was performed using EDC/NHS conjugation strategy. The availability of thiol group is critical for subsequent functionalization of nanotherapeutics yet thiol group is well-known to be very sensitive to air oxidation. Hence, CK(DUPA)GHPGGPQAsp8 was freshly activated with EDC/NHS followed by TFA deprotection and the intermediate was used directly without further purification for subsequent reaction as extensive purification procedure may cause thiol oxidation. Fortunately, small molecular weight intermediate can be easily removed by later on dialysis procedure. Tri-block copolymers were synthesized through thiol-maleimide reaction. The conjugation of peptide into PEG-PTMC block copolymers was straightforward. For example, after a

brief treatment of the peptide with tris(2-carboxyethyl) phosphine (TCEP) in phosphate buffered saline (PBS) at pH = 7.4, the peptide solution was added dropwise into Mal-PEG-block-PTMC solution in dimethyl sulfoxide, and reaction was allowed to continue overnight at 4^{o}C. Peptide-b-PEG-block-PTMC tri-block copolymer was purified by dialysis (4^{o}C), followed by ultrafiltration (MWCO = 10 K), and finally dried by lyophilization. Successful conjugation was verified by complete disappearance of the maleimide signal at σ = 6.74 ppm in ^{1}H NMR spectrum.

To better understand the potential of Pep-b-PEG-b-PTMC as a drug carrier, docetaxel (DTX) was used as a model drug to determine drug loading and release properties. DTX was encapsulated into the micelles of Pep-b-PEG-b-PTMC by a dialysis method and drug loading capacity was determined by HPLC. Pep-b-PEG-b-PTMC showed 3.16 ± 0.33 % and 31.6 ± 3.3 % for loading content and loading efficiency, respectively. As determined by dynamic light scattering, polymer micelles resulted from Pep-b-PEG-b-PTMC before DTX loading possess particle size of 47 ± 2.5 nm in diamiater. Their size increased to 65 ± 2.6 nm in diameter after DTX loading into micelles. Drug release profile in PBS buffer at pH 7.4 suggested that DTX-loaded micelles exhibited a moderately rapid release in the first stage (approximately 15 % for the first 2 hours) followed by a sustained release period. The sustained DTX release could be attributed to the hydrophobic interaction of drug molecules with the hydrophobic core of the polymeric micelles.

The strong binding ability of Pep-*b*-PEG-*b*-PTMC micelles to hydroxyapatite (HA), commonly used as a model mineral to mimic bone tissue mineral, was examined to preliminarily evaluate the contribution of peptide functionality to the bone-seeking efficacy. Cy5.5 was encapsulated into the micellar cores by the dialysis method thus to quantitatively determine the binding affinities of the nanomicelles with and without peptide functionality, respectively. After incubation for 30 min, approximately 86.2 ± 1.6% of the CK(DUPA)GHPGGPQAsp$_8$ modified NPs were rapidly bound to HA. In marked contrast, less than 10 % of MPEG-b-PTMC micelles or free Cy5.5 were bound to HA, indicating minimal nonspecific binding to HA by the MPEG-b-PTMC micelles absent of peptide functionality. Those results correlated well with the reported findings that modification with osteotropic Asp8 would dramatically facilitate the specific binding towards HA-rich bone tissue.

For the second funding period, we have been focusing on the studies of CTSK responsiveness of nanotherapeutics *in vitro*. We have also investigated and evaluated biological activities of the drug-loaded nanotherapeutics in terms of cellular uptake and tumor inhibition in cultured prostate cancer cells. Meanwhile, we have initiated bone uptake and retention of the proposed nanotherapeutics in mice.

In this project, we have hypothesized that Asp8 could be cleaved from NPs in the presence of cathepsin K, a biomarker in metastatic skeletal tissue, thus unmasking negatively charged nanotherapeutics and making DUPA ligand available to attack prostate cancer cells. In order to test our hypothesis, nanoparticles were prepared via dialysis method by using Pep-b-PEG-b-PTMC or mPEG-PTMC polymers. Cathepsin K was pre-incubated at 37°C for 5 min to activate the enzyme in the active site, followed by addition of the polymeric micelles for CTSK digestion. Surface charge and size of NPs before/after enzymatic incubation were monitored by dynamic light scattering. As shown in Figure 1, following treatment with CTSK, the zeta potential of Pep-b-PEG-b-PTMC NPs increased dramatically from -21.2 ± 0.9 mV to -2.9 ± 0.1 mV over 24-h (Figure 5 A). In contrast, the zeta potential of mPEG-b-PTMC NPs remained stable from -1.6 ± 0.7 mV to -1.8 ± 0.3 mV. There were no significant changes of the particle size during the period of enzymatic incubation of NPs (Figure 5 B),

suggesting that enzymatic digestion did not alter the integrity of NPs after Asp8 out shell removal by CTSK.

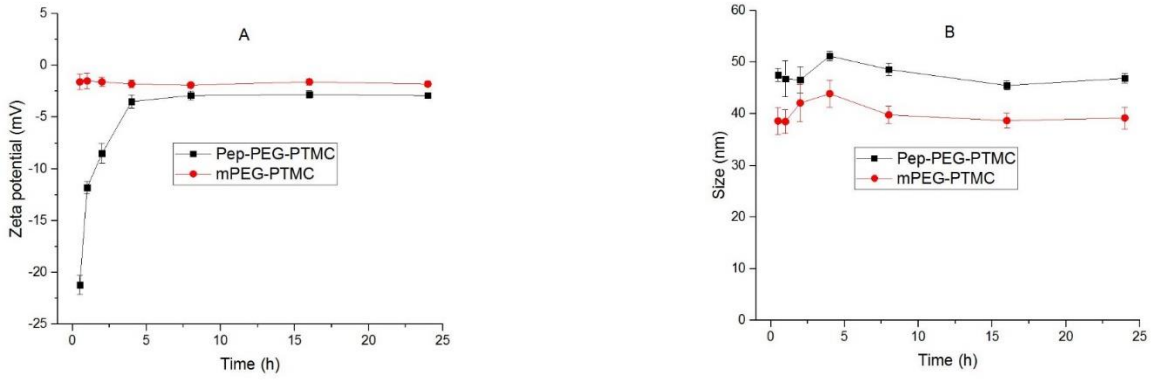

Figure 5: DLS monitoring of NPs for zeta potential (A) and particle size (B) of polymeric micelles upon co-incubation with 150 nM CTSK.

Confocal laser scanning microscopy (CLMS) was used to investigate the cellular uptake of polymeric micelles with or without CTSK treatment. The nanoparticles assembled from Pep-b-PEG-b-PTMC were loaded with Cy5.5 fluorescence indicator, followed by incubating with C4-2 prostate cancer cells in a cleavage buffer in the presence or absence of cathepsin K. Following 3-h incubation, polymeric micelles were evaluated by CLMS observation. There was little evident cellular uptake of fluorescence-labelled micelles from Pep-b-PEG-b-PTMC without CTSK treatment (Data not shown). The poor cellular uptake of untreated micelles was expected, because it was difficult for the highly negatively charged NPs to be internalized by cells. However, once these polymeric micelles were pretreated with CTSK, significant fluorescence enhancement was observed in the CLSM images (Figure 6). This was likely due to interaction between PMSA receptors in the cell membranes and DUPA ligands in NPs, thus facilitating the cellular uptake of NPs. These results indicated that nanoparticles assembled from Pep-b-PEG-b-PTMC were hardly taken up by cells. However, once the nanoparticles localize in CTSK-rich conditions, CTSK-triggered Asp8 detachment from outer shells of NPs could result in DUPA exposure to cell membrane, therefore facilitating cell entry of nanoparticles via receptor-mediated endocytosis.

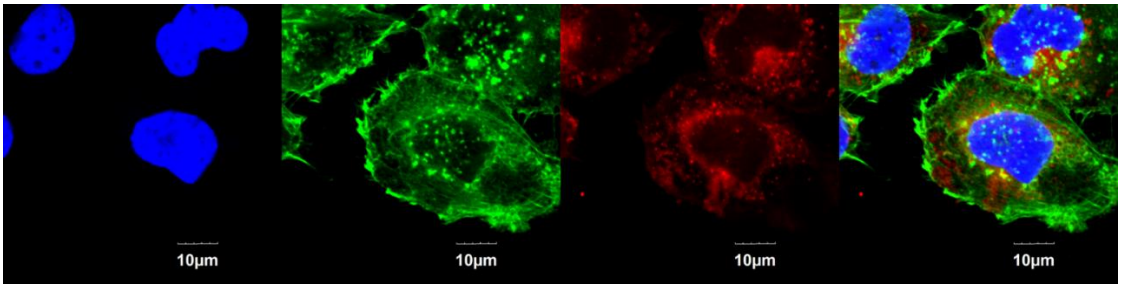

Figure 6. Cellular uptake of Cy5.5-loaded nanoparticles in C4-2 prostate cancer cells. Nanoparticles were treated with 150 nM CTSK followed by incubation with cells at 37 ºC for 3-h. Cy5.5 was shown as red fluorescence. DAPI (4',6-diamidino-2-phenylindole, blue) and Alexa Fluor®488 phalloidin (green) were used to stain cell nuclei and F-actin, respectively. Cells were imaged using a 60 × water-immersion objective.

The observation in CLSM was further confirmed by FACS analysis. Compared with the cellular uptake of nanotherapeutics without CTSK treatment, remarkably enhanced intracellular fluorescence was detected after the nanotherapeutics were pre-incubated with CTSK (Figure 7).

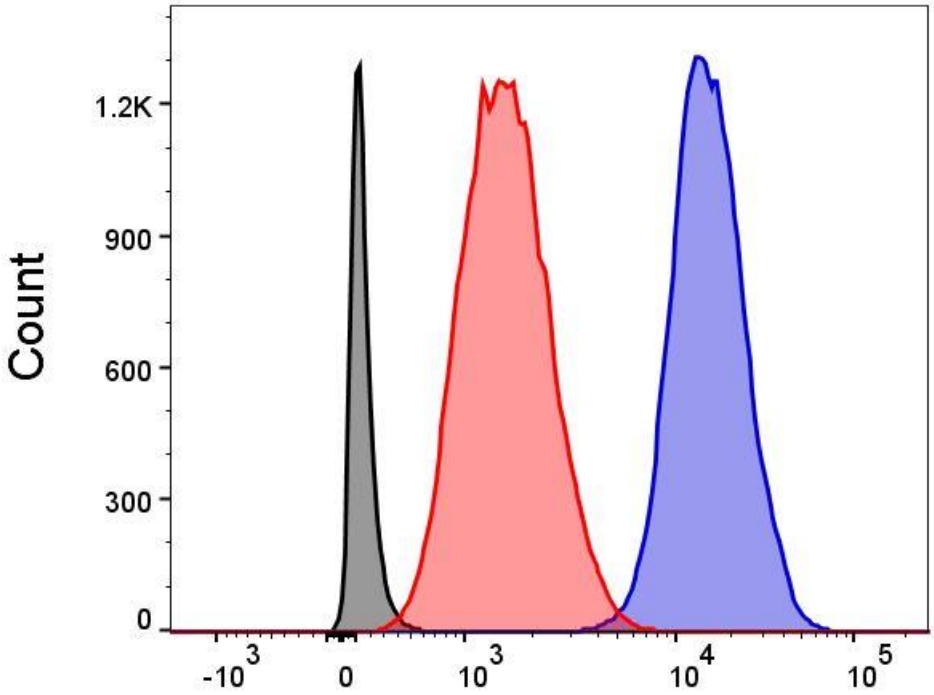

Figure 7. The fluorescent activated cell sorting (FACS) analysis of cellular uptake of Cy5.5 loaded Pep-PEG-PTMC nanoparticles after incubation with C4-2 prostate cancer cells for 3-h. Nanoparticles were pre-treated in the presence (Blue) or absence (Red) of 150 nM CTSK followed by incubation with cells at 37 ºC. Blank cells without any treatment was used as a control (Black). C4-2 cells were cultured at 37 °C, treated with NPs for 3-h, washed three times with PBS, harvested and analyzed with FACSCanto flow cytometer (BD Biosciences).

The in vitro cytotoxicity of nanotherapeutics was evaluated by measuring cell proliferation using MTT assay in cultured C4-2 prostate cancer cells. After 48-h incubation period, blank polymer without inclusion of the model drug of docetaxel (DTX) showed no detectable cytotoxicity at concentrations up to 500 $\mu g.mL^{-1}$ (Figure 8 A). In contrast, DTX-loaded nanotherapeutics exhibited considerable toxicity in the C4-2 cells with an IC_{50} at DTX concentration approximately 22.3 and 11.8 nM for Pep-PEG-PTMC and mPEG-PTMC, respectively, which was higher than that of free DTX (IC50 approximately at 7.2 nM) (Figure 8 B). Cell proliferation assay was also carried out when nanotherapeutics were firstly treated with 150 nM CTSK, followed by cell viability experiments. No difference was observed in the cases of free DTX or DTX-loaded nanotherapeutic by using mPEG-PTMC as the drug carrier. Interestingly, improved tumor inhibition was observed for peptide functionalized nanotherapeutics. For example, in the case of Pep-PEG-PTMC based DTX-loaded nanotherapeutics, tumor cells growth inhibition of C4-2 cells was determined as 65.7%, 42.3% and 32.7% at DTX concentration of 6.25, 25 and 100 nM, respectively. When the nanotherapeutics were pre-incubated with CTSK, the tumor cells growth inhibition of C4-2 cells was improved as 51.9%, 33.3% and 19.9% at DTX concentration of 6.25, 25 and 100 nM, respectively. (Figure 8 C). These

results indicated that the drug sensitivity of peptide functionalized nanotherapeutics can be improved in a CTSK-rich microenvironment. As the progression and bone metastasis of prostate cancer are positively correlated with expression of CTSK, it is expected that CTSK-responsive nanotherapeutics are promising for advanced prostate cancer therapy.

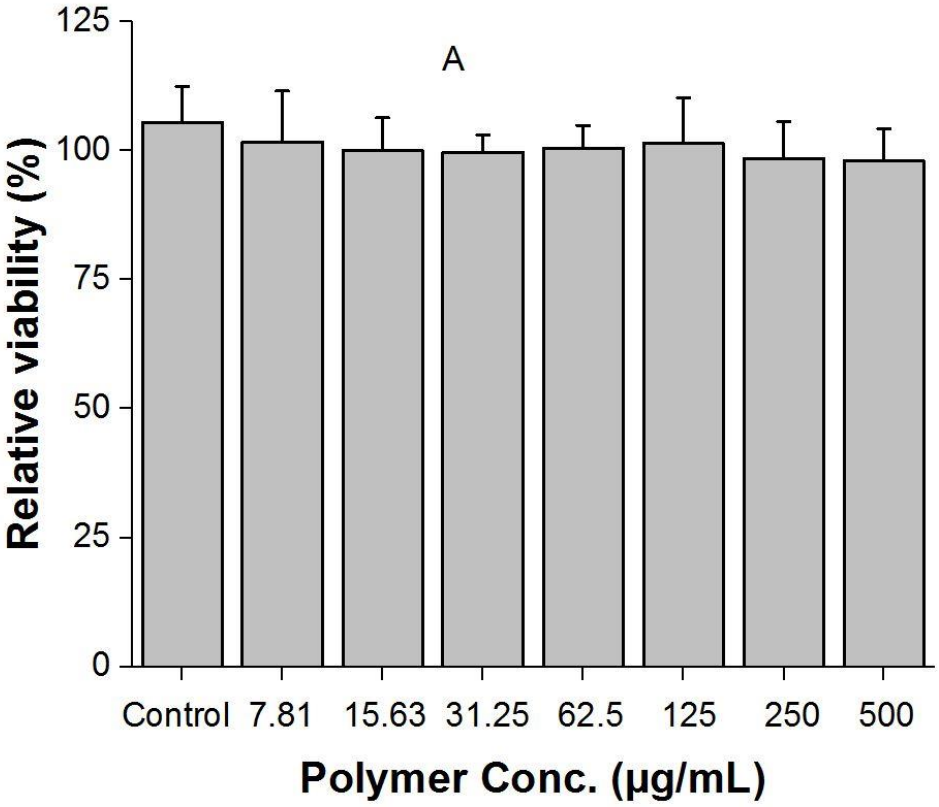

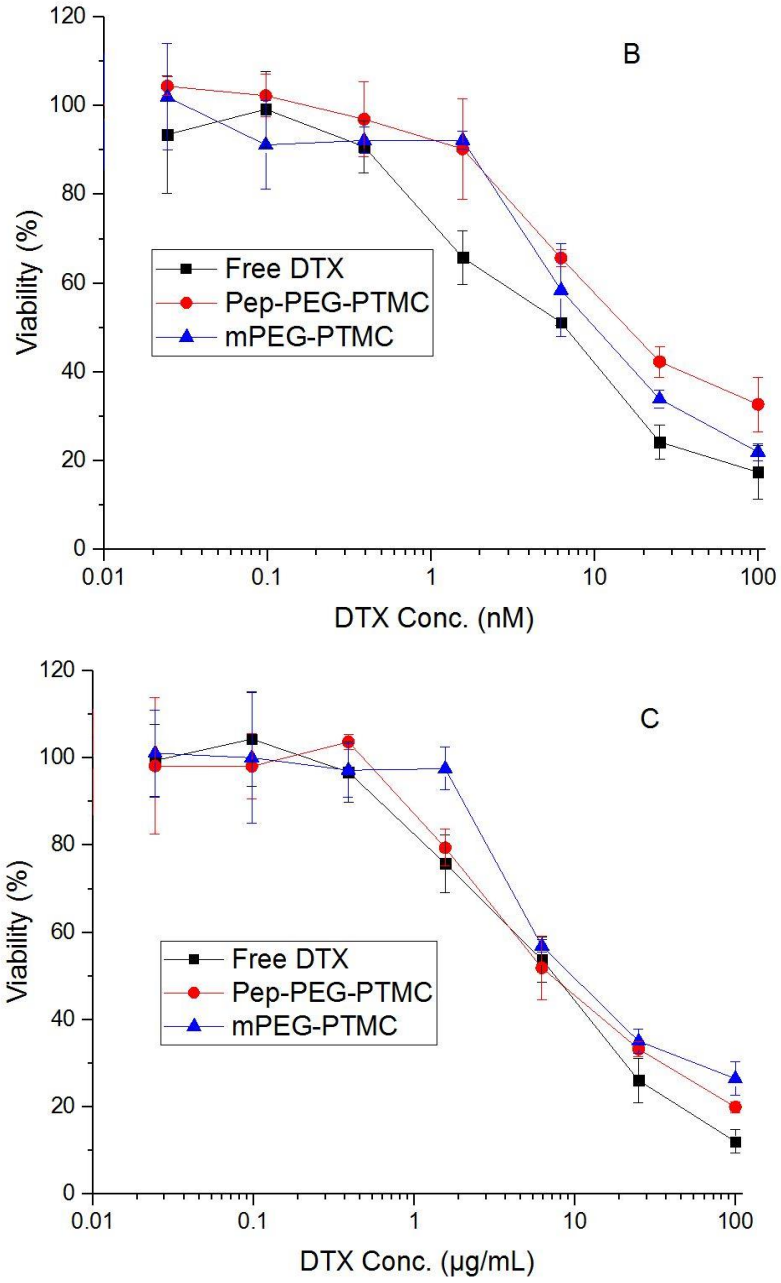

Figure 8: Cell viability of C4-2 prostate cancer cells after treatment with blank copolymer of Pep-PEG-PTMC (A). Cell viability of 4C-2 prostate cancer cells after treatment with free DTX or DTX-loaded copolymer of Pep-PEG-PTMC or mPEG-PTMC (B). Free DTX or DTX-loaded copolymer of Pep-PEG-PTMC or mPEG-PTMC was firstly treated with 150 nM CTSK followed by incubation with 4C-2 prostate cancer cells to determine cell viability by MTT assay (C).

The strong binding ability of Pep-*b*-PEG-*b*-PTMC micelles to hydroxyapatite (HA) has been confirmed that nearly 90% of the CK(DUPA)GHPGGPQAsp$_8$ modified NPs were rapidly bound to HA. In marked contrast, less than 10 % of mPEG-b-PTMC micelles were bound to HA, indicating minimal nonspecific binding to HA by the mPEG-b-PTMC micelles absent of peptide functionality. We have further studied bone uptake and retention of the nanotherapeutics in animals by using non-invasive optical imaging modality. Cy5.5 was used as a near infrared fluorescent (NIRF) optical imaging agent. Bone-targeted Cy5.5-loaded NPs were prepared using Pep-PEG-PTMC as the drug carrier. Equivalent dose of NIRF probe (2 nmol) was administered into mice via tail vein injection, and the preferential bone-tissue accumulation of Cy5.5 was clearly observed by near-infrared fluorescence imaging using bone-targeted nanocarrier in vivo and ex vivo (Figure 9). The results demonstrated that modification with osteotropic Asp8 would dramatically facilitate the specific binding towards bone tissue. This bodes well for bone-targeting capacity of nanotherapeutics *in vivo*, and more detailed examination of bone-related therapeutic evaluation will be performed in the next funding period.

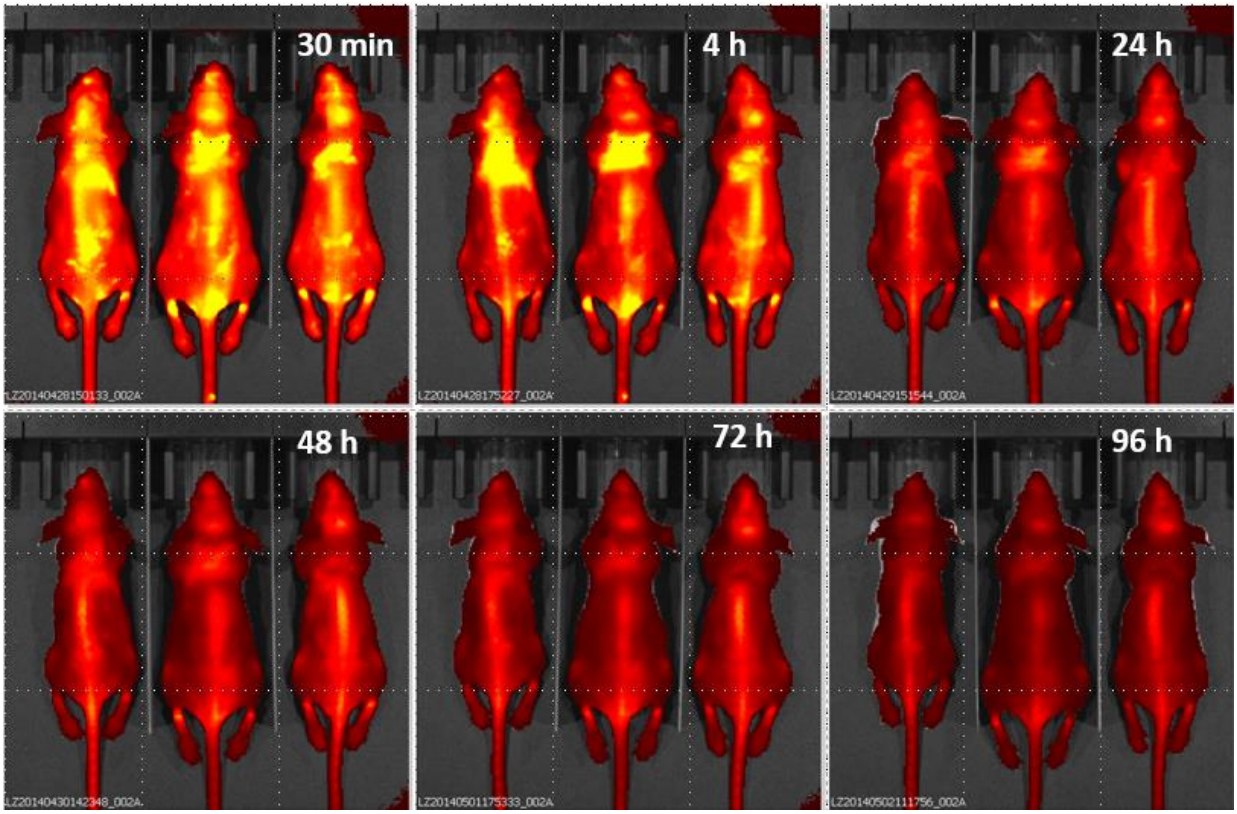

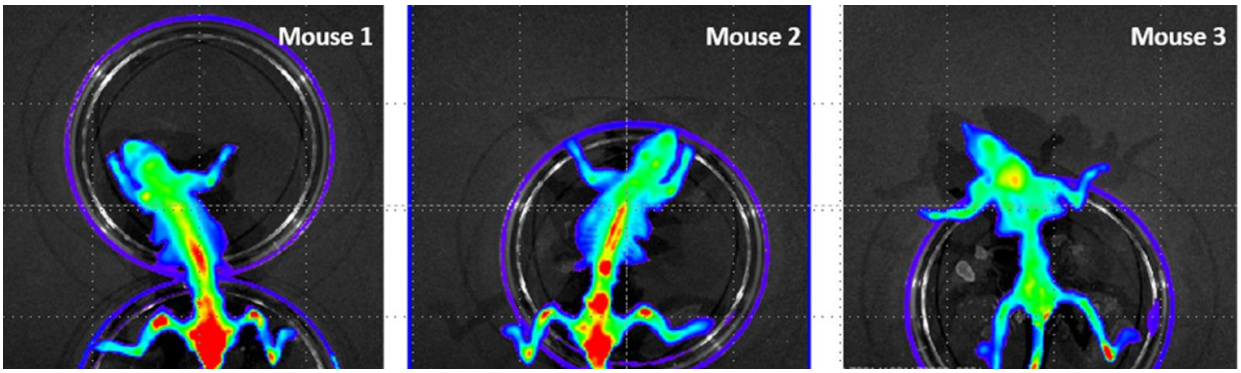

Figure 9: Athymic nude mice (Nu/Nu strain) were used for non-invasive optical imaging studies. For near-infrared fluorescence (NIRF) imaging, nude mice were intravenously injected with equivalent amount of 2 nmol Cy5.5 of bone-targeted Cy5.5-loaded NPs. At different time points post injection of imaging probe, mice were scanned using an IVIS Spectrum Pre-clinical In Vivo Imaging System (Perkim Elmer, USA) with an excitation bandpass filter at 670 nm and an emission at 720 nm. The mice were anesthetized by isoflurane during each imaging procedure. Results were analyzed using Living Image 4.4 software (Perkim Elmer, USA). After 96-h post injection of NPs, mice were sacrificed and ex vivo optical imaging was acquired to further validate that the imaging probes were indeed accumulated in hard tissues.

In order to identify promising nanotherapeutics for future preclinical investigation in animals, the biological performance in terms of tumor inhibition of nanotherapeutics has been evaluated in three human prostate cancer cell lines, i.e. LNCaP, C4-2B and PC3 cells. The characteristics of these cells are summarized in Table 1. Briefly, LNCaP are PSMA positive, androgen-dependent prostate cancer cells but they are generally lack of metastatic capability. C4-2B, a LNCaP derivative cell line, are PSMA-positive, highly tumorigenic, androgen-independent cells which are able to develop osteoblastic skeletal metastases. PC3 are PSMA-negative, androgen-independent prostate cancer cells which are able to develop osteolytic skeletal metastases. As shown in Table 1, DTX loaded nanotherapeutics with Pep-PEG-PTMC generally were less toxic in LNCaP and C4-2B cells than that of mPEG-PTMC or free DTX. However, in the case of PC3 cells, it was interesting that nanotherapeutics from Pep-PEG-PTMC (IC_{50} = 56.3 ± 3.7 nM) mediated comparable cytotoxicity as free DTX (IC_{50} = 51.8 ± 2.8 nM), and much more potent tumor inhibition than that of mPEG-PTMC (IC50 = 116.3 ± 4.5 nM). It is speculated that the osteolytic feature of PC3 cells by overexpression of CTSK may facilitate the removal of Asp8 moiety, thus unmasking negatively charged nanotherapeutics to enhance their tumor uptake and then attack prostate cancer cells.

Table 1: Tumor inhibition of nanotherapeutics in different prostate cancer cell lines

Cell line	Origin (species)	PSMA status	Metastatic capability	Bone lesion	IC50 (nM)		
					Free DTX	mPEG-PTMC/DTX	Pep-PEG-PTMC/DTX
LNCaP	Human	Positive	No	N.A	4.1 ± 0.8	8.6 ± 0.7	9.3 ± 2.2
C4-2B	Human	Positive	Yes	osteoblastic	7.2 ± 1.1	11.8 ± 1.5	22.3 ± 1.6
PC3	Human	Negative	Yes	osteolytic	51.8 ± 2.8	116.3 ± 4.5	56.3 ± 3.7

The next step was to establish PC3 cells induced bone metastatic animals. There are several practical mouse models to induce bone metastasis, such as inoculation of cancer cells into orthotropic locations, bones, or direct injection of cancer cells into mice. In this project we established the animals with bone metastasis by injecting prostate cancer cells (PC-3-Luc) through the left ventricle of the heart followed by monitoring the progress cancer induced bone metastases with bioluminescence imaging modality. We have considered using this bone metastatic animal model because: 1): The method to establish such an animal model of bone metastasis from prostate cancer is established in literature. 2) PC3 prostate cancer cells are able to develop osteolytic skeletal metastases. 3) Interactions of PC3 cells with osteoclasts reportedly lead to cathepsin K up-regulation, resulting in osteolytic lesions. 4) As aforementioned, the in vitro results have demonstrated the therapeutic advantages of nanotherapeutics from Pep-PEG-PTMC over that of mPEG-PTMC, providing rationale to test nanotherapeutics in PC3 cells induced bone metastatic animals.

It was very challenging to perform intra-cardiac injection procedure, which was the most critical step in order to obtain prostate cancer induced bone metastatic animals. The procedure was described as the following: A 29-gauge needle and a 0.5 cc syringe loaded with 2 million PC-3 cells in PBS (100 µL total volume) were used for injection (Figure 10 A). It was important to inject the needle directly into the chest between the animal's sternum and third intercostals space, inserting the needle into the second intercostals space, and making sure to inject the cells into the left ventricle of the heart. When inserting the needle into the left ventricle of the heart properly, blood will pump into syringe needle. When this happens, it is time to begin to inject the cell solution by using a very slow pace (approximately 30 seconds for total 100 µL). Injecting too fast is prohibited which can kill the animal instantly due to the arteries being clogged. Once the injection is complete, the needle needs to be taken directly straight out quickly. After the injection is complete and successful, bioluminescence imaging is acquired to confirm the success of tumor cells injection via intracardiac injection as mentioned above. After bioluminescence imaging acquisition (several minutes) is done, the animal was placed back into a clean cage, which was left onto the heating pad until the animal fully recovered from the anesthesia and was walking around the cage. The animal should be monitored closely until has done so. Bioluminescence Imaging: After 2 million PC-3-Luc cells were injected in 100 µL volume in to the left ventricle, a dose of 150 µg D-luciferin in PBS is injected into mouse via IP to validate injection technique. To confirm a correct intracardiac injection, mice should be imaged in the IVIS system right after injection. Mice that show BLI signal throughout the body have been injected correctly (Figure 10 (B)). If signal was localized, it indicated that the cells were not injected correctly into the heart. Typically, 3 weeks after intracardiac injection of tumor cells resulted in extensive bone metastases in animals (Figure 10 (C)). For drug efficacy studies, three days after successful intracardiac injection of PC3 cells, mice were randomly grouped (5 per group), and treatment experiments were initiated. DTX-loaded, functional nanotherapeutics which is identified in previous sections as well as its corresponding non-functional NPs, free DTX, were tested and PBS was used as a control. The doses of DTX (10 $mg.Kg^{-1}$) were kept consistent in different groups. Our preliminary *in vivo* test indicated that mice treated with the DTX-loaded nanotherapeutics had prolonged survival rates when compared to mice treated with free DTX. More importantly, DTX-loaded, peptide functionalized NPs were more efficacious in terms of survival than those treated with non-functional NPs, free DTX or PBS control (Figure 10 D). This improved drug efficacy may be attributed to more selective delivery of DTX to bone metastatic tissues and/or responsiveness of the NPs to CTSK, thus improving tumor uptake of DTX, enhancing therapeutic efficacy in terms of tumor reduction as well as survival.

(A)

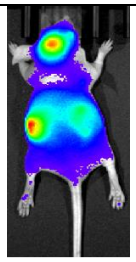

(B)

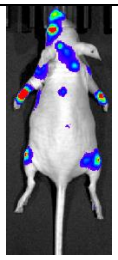

(C)

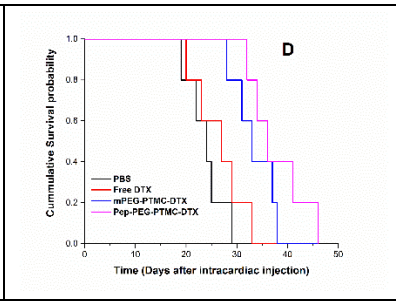

Figure 10. A prostate cancer induced bone metastatic animal was established by using a intracardiac injection route (A). Successful intracardiac injection of tumor cells showed BLI signal throughout the body (B). 21-day after intracardiac injection of PC3 cells into mouse induced extensive bone metastases in animals (C). Efficacy of free DTX or DTX-loaded NPs in PC3 cells induced bone metastatic animals. Bone metastatic animals were established through intracardiac injection of PC3-Luc cells (2×10^6 cells in 100 μL PBS), and tumor was allowed to grow for 3-d before initiating treatment study. Mice (5 per group) were injected weekly with different therapeutic formulations at equivalent DTX dose (10 mg/Kg) or PBS (D).

In summary, we have performed extensive studies with very encouraging results in the development of nanotherapeutics for prostate cancer therapy. We have established practical procedures for synthetic chemistry and nanotherapeutic formulation, and further demonstrated some key features of the nanotherapeutics, such as bone binding affinity, CTSK-responsiveness, and anti-tumor activity in vitro and in vivo. Our research indicates our proposed bone specific therapeutic platform for bone metastatic cancer therapy is feasible, practicable and applicable. These results have strongly motivated us to pursue the further development (through intramural and extramural supports) of nanotherapeutics in hopes of improving therapy of cancer induced bone metastases, including but is not limited advanced prostate cancer.

What opportunities for training and professional development has the project provided?

"Nothing to Report."

How were the results disseminated to communities of interest?

"Nothing to Report."

What do you plan to do during the next reporting period to accomplish the goals?

"Nothing to Report."

4. **IMPACT:**

What was the impact on the development of the principal discipline(s) of the project?

"Nothing to Report."

What was the impact on other disciplines?

"Nothing to Report."

What was the impact on technology transfer?

"Nothing to Report."

What was the impact on society beyond science and technology?

"Nothing to Report."

5. **CHANGES/PROBLEMS:**

"Nothing to Report"

Changes in approach and reasons for change

"Nothing to Report"

Actual or anticipated problems or delays and actions or plans to resolve them

"Nothing to Report"

Changes that had a significant impact on expenditures

"Nothing to Report"

Significant changes in use or care of human subjects, vertebrate animals, biohazards, and/or select agents

"Nothing to Report"

6. **PRODUCTS:**

Manuscript:

Xuli Wang, Ye Yang, Huizhen Jia, Wanjian Jia, Scott Miller, Beth Bowman, Jun Feng and Fenghuang Zhan, Peptide decoration of nanovehicles to achieve active targeting and pathology-responsive cellular uptake for bone metastasis chemotherapy, *Biomaterials Science*, **2014**, 2, 961-971

One manuscript is in preparation.

Abstract:

Xuli Wang, Le Zhan, Tao Liu and Garrison Colvin, Design and Development of Prostate Cancer-Responsive Nanotherapeutics, 2016 Innovative Minds in Prostate Cancer Today (IMPaCT) Meeting (IMPaCT 2016), August 3-5, Baltimore, Maryland

7. **PARTICIPANTS & OTHER COLLABORATING ORGANIZATIONS**

What individuals have worked on the project?

Name:	Xuli Wang, Ph.D.
Project Role:	Principal Investigator
Nearest person month worked:	4
Contribution to Project:	Responsible for the overall management of the project. Dr. Wang has also involved in chemical synthesis for this project.
Funding Support:	This award and support from NCI
Name:	Mary Beth Bowman
Project Role:	Technician
Nearest person month worked:	3
Contribution to Project:	Ms. Bowman has performed work in the area of investigation and evaluation of nanotherapeutics.
Funding Support:	This award.
Name:	Le Zhan
Project Role:	Graduate Student

Nearest person month worked:	6
Contribution to Project:	Ms. Zhan has performed work in the area of investigation and evaluation of nanotherapeutics.
Funding Support:	This award.
Name:	Tao Liu
Project Role:	Graduate Student
Nearest person month worked:	5
Contribution to Project:	Mr. Liu has performed work in the area of chemical synthesis and characterization of nanotherapeutics.
Funding Support:	NCI
Name:	Garrison Colvin
Project Role:	Undergraduate Student
Nearest person month worked:	1
Contribution to Project:	Mr. Colvin has performed work in the area of chemical synthesis and characterization of nanotherapeutics.
Funding Support:	This award.

Has there been a change in the active other support of the PD/PI(s) or senior/key personnel since the last reporting period?

"Nothing to Report."

What other organizations were involved as partners?

"Nothing to Report."

8. **SPECIAL REPORTING REQUIREMENTS**

N.A.

9. **APPENDICES:**

A manuscript and a meeting abstract have been attached.

Volume 2 | Number 7 | July 2014 | Pages 945–1036

Biomaterials Science

www.rsc.org/biomaterialsscience

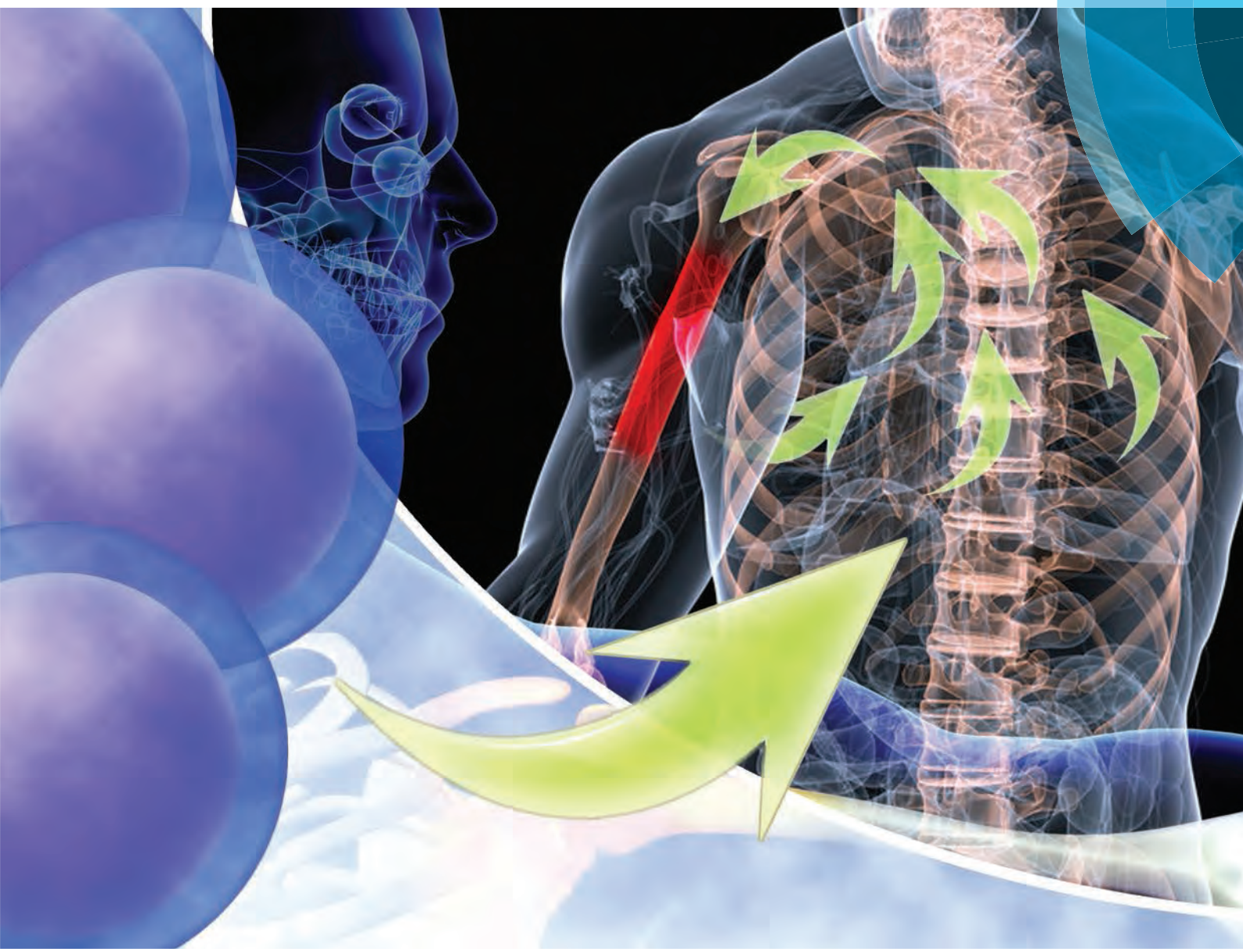

ISSN 2047-4830

ROYAL SOCIETY OF CHEMISTRY

PAPER
Xuli Wang, Jun Feng, Fenghuang Zhan *et al.*
Peptide decoration of nanovehicles to achieve active targeting and pathology-responsive cellular uptake for bone metastasis chemotherapy

iCeMS KYOTO UNIVERSITY WPI Research Center

Biomaterials Science

PAPER

View Article Online
View Journal | View Issue

Cite this: *Biomater. Sci.*, 2014, **2**, 961

Peptide decoration of nanovehicles to achieve active targeting and pathology-responsive cellular uptake for bone metastasis chemotherapy†

Xuli Wang,*‡[a] Ye Yang,‡[b] Huizhen Jia,[c] Wanjian Jia,[a] Scott Miller,[a] Beth Bowman,[a] Jun Feng*[c] and Fenghuang Zhan*[b]

Received 19th January 2014,
Accepted 11th March 2014

DOI: 10.1039/c4bm00020j

www.rsc.org/biomaterialsscience

To improve bone metastasis chemotherapy, a peptide-conjugated diblock copolymer consisting of a chimeric peptide, poly(ethylene glycol) and poly(trimethylene carbonate) (Pep-*b*-PEG-*b*-PTMC) is fabricated as a drug carrier capable of bone-seeking as well as pathology-responsive charge reversal to ensure effective cellular uptake at the lesion sites. The chimeric peptide CKGHPGGPQAsp$_8$ consists of an osteotropic anionic Asp8, a cathepsin K (CTSK)-cleavable substrate (HPGGPQ) and a cationic residue tethered to the polymer chain. Pep-*b*-PEG-*b*-PTMC can spontaneously self-assemble into negatively charged nanomicelles (~75 nm). As to the model drug of doxorubicin, Pep-*b*-PEG-*b*-PTM shows 30.0 ± 1% and 90.1 ± 2% for the loading content and loading efficiency, respectively. High bone binding capability is demonstrated with 66% of Pep-*b*-PEG-*b*-PTMC micelles were able to bind to hydroxyl apatite, whereas less than 15% of Pep-free micelles were bound to hydroxyl apatite. The nanomicelles exhibit a negative-to-positive charge conversion from –18.5 ± 1.9 mV to 15.2 ± 1.8 mV upon exposure to CTSK, an enzyme overexpressed in bone metastatic microenvironments. Such a pathology-responsive transition would lead to remarkably enhanced cellular uptake of the nanomicelles upon reaching lesion sites, thus improving the drug efficacy as verified by the *in vitro* cytotoxicity assay and the *in vivo* study with the myeloma-bearing 5TGM1 mice model.

1. Introduction

Most patients with cancer die not because of the tumor in the primary site, but rather because it spread to other sites of which the bone is the most common organ to be affected.[1,2] Patients with bone metastases generally cannot be treated curatively, *e.g.*, only 20% of patients with breast cancer remain alive for five years after the diagnosis of bone metastases; more than 550 000 people die annually with bone metastases.[1,3] Effective chemotherapy of bone metastases has therefore remained an urgent challenge for cancer treatments.[4]

The surface decoration of drug nanovehicles (NVs) with bone-targeting moieties is among the most used strategies to improve the chemotherapy against bone metastases.[5] Given the remarkable feature of skeletal tissue rich in apatite ($Ca_{10}(PO_4)_6$), many anionic agents with high apatite binding affinity including bisphosphonates (BPs) and oligopeptides (Asp_6, Asp_8 and Glu_8) have been purposely incorporated into NVs for the sake of bone-seeking action.[5–7] However, the treatment efficacies achieved by those bone-targeting NVs are still far from satisfactory; some of them were even less efficacious than the unmodified counterparts. The marked deviation from the expectation is thought to be associated with the dilemma that the attachment of anionic agents to NVs inevitably restricts cellular translocation due to the charge repulsion by the cell membranes.[4–6] In turn it is difficult for the drugs loaded into NVs to enter cancerous cells to elicit therapeutic action. In contrast, despite the easy intracellular internalization, the applications of positively charged NVs suffer a lot from rapid *in vivo* clearance and non-specific uptake by healthy tissues resulting from the strong interaction with oppositely charged blood components and the cell membranes. Taking those into account, the solution to bone-targeted chemotherapy may eventually rely on the rational design of anionic bone-seeking NVs which are simultaneously capable of undergoing negative-to-positive charge transition that mostly occurs in bone metastatic sites.

[a]*Division of Radiobiology, School of Medicine, University of Utah, 729 Arapeen Drive, Rm 2334, Salt Lake City, 84108, USA. E-mail: xuli.wang@utah.edu*
[b]*Department of Internal Medicine, Division of Hematology, Oncology, and Blood & Marrow Transplant, University of Iowa, Iowa City, IA 52242, USA. E-mail: fenghuang-zhan@uiowa.edu*
[c]*Key Laboratory of Biomedical Polymers of Ministry of Education & Department of Chemistry, Wuhan University, Wuhan 430072, China. E-mail: fengjun@whu.edu.cn*
†Electronic supplementary information (ESI) available. See DOI: 10.1039/c4bm00020j
‡These authors contributed equally.

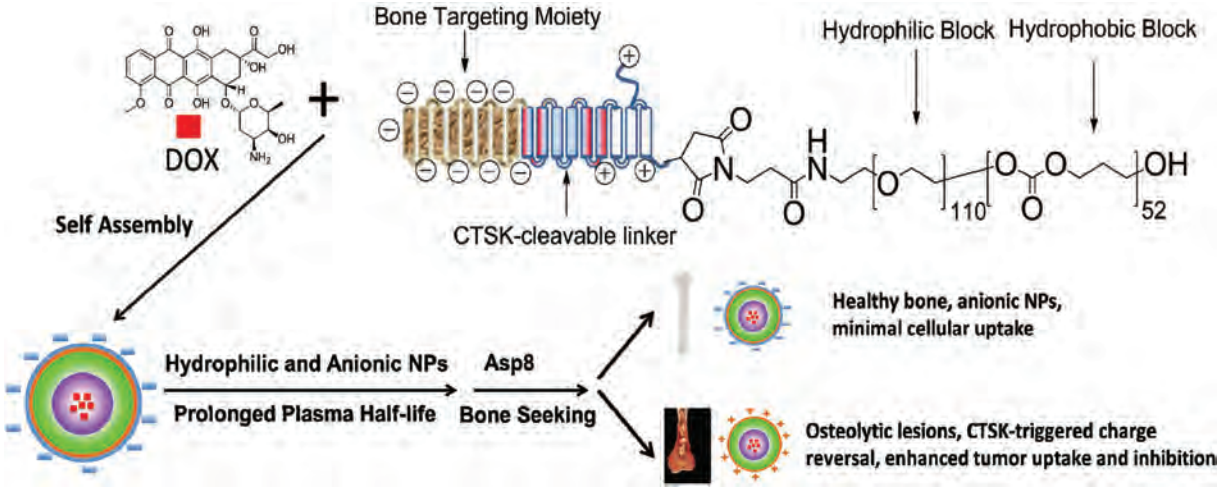

Scheme 1 Schematic illustration of nanotherapeutic formation and its mechanism of action *in vivo* for bone metastasis treatment.

One notable physicochemical feature of bone metastases is the predominant over-expression of several proteases including matrix metalloproteinase, urokinase plasminogen activator, and cathepsins (cathepsins K, L, and B).[8] In particular, the development of cancer metastases in bones is found to be highly correlated with the expression level of the acid-activated cathepsin K enzyme (CTSK). The bone metastatic lesions express even dramatically higher level of CTSK compared to primary tumor and soft tissue metastases.[9] The strong dependence of bone metastases on the CTSK level makes CTSK able to serve as a prognostic indicator for the diagnosis of bone metastases and as a therapeutic target for disease treatments.[10–12] This pathology-dependent feature of CTSK overexpression evokes our interest to exploit CTSK as the biological stimulus to locally trigger the charge reversal of anionic bone-seeking NVs upon reaching bone metastatic sites.[13–16]

We have herein designed a bone-seeking, CTSK-responsive charge-reversal NV system for efficient chemotherapy of bone metastases. This delivery system was constructed on the core–shell nanomicelles self-assembled from a triblock copolymer (Pep-*b*-PEG-*b*-PTMC) composed of a peptide segment with the sequence CKGHPGGPQAsp$_8$, poly(ethylene glycol) and poly(trimethylene carbonate). The chimeric peptide segment consisted of three main functional modules: the anionic Asp$_8$ is responsible for the direction and accumulation of NVs into the skeletal tissues, the HPGGPQ serves as the CTSK-cleavable substrate,[8] and the remaining cationic residue is chemically conjugated to the PEG shell of the micelles. In this way, the combination of the targeting function of Asp$_8$ and the stealth effect of the PEG shell would help the drug-loaded Pep-*b*-PEG-*b*-PTMC nanomicelles prolong the circulation time and minimize the undesirable cellular uptake by healthy cells. Of special note is that the bone metastatic microenvironment featured with CTSK overexpression would locally stimulate the enzymatic cleavage of HPGGPQ moieties, leaving the cationic peptide residue on the shell periphery. This pathology-responsive charge reversal transition is expected to largely contribute to the selectively efficient internalization of nanomicelles into the neighboring cancerous cells (Scheme 1), thus improving the therapeutic efficacy. In principle, this strategy of bone-seeking, pathology-responsive charge-reversal NVs may be also applicable to other malignant diseases of skeletal tissue if the development of those diseases involves overexpression of certain enzymes. To verify our hypothesis, an anticancer drug DOX was used as the drug model and the *in vitro* and *in vivo* properties of the Pep-*b*-PEG-*b*-PTMC nanomicelles were comparatively explored under the CTSK-rich and CTSK-absent conditions.

2. Experimental section

2.1. Materials

Monomethyl terminated polyethylene glycol monoamine (MeO-PEG$_{113}$-OH, M_w = 5000 Da) was purchased from Sigma-Aldrich. It was dried by azeodistillation of anhydrous benzene prior to use. Heterofunctional PEG with monomaleimide and monohydroxyl terminus (Mal-PEG$_{110}$-OH, M_w = 5000 Da) was purchased from Laysan Bio (Arab, AL) and dried under high vacuum. Trimethylene carbonate (TMC) was prepared as previously described.[17] It was recrystallized from a THF–ether mixture, and further purified *via* sublimation prior to use. 1,8-Diazabicyclo[5.4.0]undec-7-ene (DBU) was distilled from CaH_2 under dry N_2 prior to use. The *N*-(3,5-trifluoromethyl)phenyl-*N*-cyclohexylthiourea (TU) catalyst was prepared as described elsewhere.[18] Stannous octoate (Sn(Oct)$_2$, Sigma) was purified according to a method described in the literature.[19] Anhydrous solvents were purchased from Sigma-Aldrich and stored over molecular sieves (4 Å). Doxorubicin was purchased from Selleck Inc. (Houston, TX). Cy5.5 was purchased from Lumiprobe (Russia). Cathepsin K was purchased from EMD Biosciences. Hydroxyapatite (HA) was purchased from Bio-Rad (Bio-Gel HTP, DNA grade; Hercules, CA). 1-Hydroxybenzotriazole (HOBt), *O*-benzotriazole-*N*,*N*,*N*′,*N*′-tetramethyl-uronium-

hexafluoro-phosphate (HBTU), Rink amide resin, NovaSyn TGT alcohol resin and all of the amino acids for solid phase peptide synthesis were purchased from Novabiochem (CA). All other chemical reagents were available commercially and used as received unless otherwise noted.

2.2. Peptide synthesis

ISOLUTE column reservoirs (Charlottesville, VA) were used for the solid phase synthesis. The functional peptide with the sequence of CKGHPGGPQAsp$_8$ was synthesized by a standard solid phase peptide synthesis (SPPS) procedure by using the Rink amide resin solid support and HBTU/HOBt as coupling reagents. Coupling efficiencies were monitored by the Kaiser ninhydrin test. The peptide was cleaved from the resin by treatment with the TFA–EDT–H_2O–TIBS (94/2.5/2.5/1) mixture as a scavenger. The crude was precipitated with cold ethyl ether and purified by preparative RP-HLPC. The purity of the peptide was checked by analytical RP-HPLC and the molecular weight was confirmed by MALDI-TOF mass spectrometry, MS (m/z, $[M]^+$): 1800.68 (calculated for $C_{68}H_{97}N_{21}O_{35}S$); 1800.54 (found).

2.3. Synthesis of the MPEG-*b*-PTMC di-block copolymer (MPEG-*b*-PTMC)

HO-PEG$_{113}$-OMe (5 g, 1 mmol), TMC (5.1 g, 50 mmol) and TU (380.6 mg, 2.5 mmol, 5 mol% of TMC monomer) were dissolved in 25 mL dichloromethane (DCM), and then DBU (380.6 mg, 2.5 mmol, 5 mol% of TMC monomer) was added. The reaction was performed under a N_2 atmosphere for 24 hours. The reaction mixture was concentrated under a reduced pressure and the product was obtained by precipitation in ether. The residue was re-dissolved in a minimal amount of DCM and then poured into cold ether to precipitate the product; total yield: 8.6 g (85.2%).

2.4. Synthesis of the maleimide-terminated PEG-*b*-PTMC polymer (Mal-PEG-*b*-PTMC)

Mal-PEG$_{110}$-*b*-PTMC$_{52}$ was synthesized by ring-opening polymerization using Mal-PEG$_{110}$-OH (0.5 g) as the initiator, Sn(Oct)$_2$ as the catalyst and anhydrous toluene as the solvent. The reaction was performed at 100 °C under a N_2 atmosphere for 16 hours. The reaction mixture was concentrated under a reduced pressure and the product was obtained by precipitation in ether. The residue was re-dissolved in a minimal amount of THF and then poured into cold ether to precipitate the product. Yield: 0.72 g (71.3%).

2.5. Synthesis of the peptide-*b*-PEG-*b*-PTMC copolymer (peptide-*b*-PEG-*b*-PTMC)

Peptide (CKGHPGGPQAsp$_8$, 50 mg, 27.8 μmol) was dissolved in PBS buffer (pH = 7.2) and treated with tris(2-carboxyethyl) phosphine (TCEP, 40 μmol) for 2 hours under a N_2 atmosphere. After that, 213 mg of Mal-PEG-*b*-PTMC in 5 mL of dimethylacetamide (DMAc) was added. The reaction was performed at room temperature overnight. The reaction mixture was then subject to dialysis against water (MWCO = 6–8 kDa, Spectrumlabs) at 4 °C for 24 hours. The solution was further purified using Microsep™ Centrifugal Devices with the Omega™ Membrane (MWCO = 10 kDa, Pall Life Sciences). The final product was recovered and dried by lyophilization. Yield: 151 mg (57.5%).

2.6. NMR characterization

The MERCURY 400 MHz spectrometer was used for recording ^{1}H NMR spectra to determine the structure and composition of the block copolymers. Deuterium oxide (D_2O), deuterated chloroform ($CDCl_3$) and dimethyl sulfoxide (DMSO-d_6) were used as the solvents as noted for NMR measurements.

2.7. Determination of critical micelle concentration (CMC)

Critical micelle concentrations of the copolymers were estimated by a fluorescence spectroscopy method using pyrene as the fluorescence probe.[20] A predetermined amount of pyrene solution in acetone was added into a series of volumetric flasks, and the acetone was then evaporated completely. A series of copolymer solutions of different concentrations ranging from 1.0×10^{-5} to 1.0 mg mL^{-1} were added to the bottles, whereas the concentration of pyrene in each flask was fixed at a constant value (6.0×10^{-7} mol L^{-1}). The excitation spectra were recorded at 20 °C on a Shimadzu RF-5301PC spectrofluorophotometer with the detection wavelength at 390 nm and a slit width of 3 nm. The intensity ratio of the bands at 340 and 338 nm (I_{340}/I_{338}) as a function of the logarithm of the concentration of copolymers was plotted and the CMC value was taken as the intersection of the tangents to the horizontal line of the intensity ratio with relatively constant values and the diagonal line with rapid increased intensity ratio.

2.8. Preparation of self-assembled nanoparticles

2.8.1. Preparation of blank nanoparticles. Blank micelles were prepared by a dialysis method. Briefly, the block copolymer (10 mg) was dissolved in 1 mL of DMSO and stirred for 10 min at room temperature. Then, 5 mL of double distilled water was added dropwise into the polymer solution under stirring. After 30 min, the solution was transferred into a dialysis membrane tubing (MWCO = 6–8 kDa, Spectrumlabs) and dialyzed for 24 h against distilled water to remove the organic solvent. The solution was recovered and lyophilized to afford blank nanoparticles.

2.8.2. Preparation of fluorescence-labeled nanoparticles. In order to track nanoparticles, fluorescence-labeled nanoparticles were prepared using Cy5.5 as a fluorescent tracer. Cy5.5-labeled nanoparticles were similarly prepared following the above-described dialysis method.

2.8.3. Preparation of DOX-loaded NVs. Unless otherwise noted, all procedures for preparation and handling of DOX-loaded NVs were performed in the dark. DOX-loaded micelles were prepared similarly to the blank micelles. Briefly, 10 mg of each polymer was dissolved in 1 mL of DMSO, followed by adding a predetermined amount of DOX·HCl and two molar equivalents of triethylamine (TEA) and stirred at room temp-

erature for 1 h. Then, 5 mL of double distilled water was added dropwise. After being stirred for an additional 1 h, the solution was dialyzed (MWCO = 6–8 kDa, Spectrumlabs) against water for 24 h. Drug-loaded NVs were dried *via* lyophilization.

2.9. Determination of drug loading capacity

The drug loading content was determined spectrophotometrically by measuring the absorption of the lyophilized sample which was dissolved in DMSO at a wavelength of 482 nm. The absorbance of DOX in nanoparticles was measured to determine the drug content in the solution using an established calibration curve with a known concentration of free DOX. The percentages of DLC (drug loading content) and DLE (drug loading efficiency) were calculated according to the following equations:

$$\mathrm{DLC}\,(\%) = \frac{\text{amount of DOX in micelle}}{\text{amount of DOX-loaded micelles}} \times 100\%$$

$$\mathrm{DLE}\,(\%) = \frac{\text{amount of DOX in micelle}}{\text{amount of DOX used for nanomicelle preparation}} \times 100\%$$

2.10. Drug release profile

Drug release experiments were performed in a buffer with a fixed ionic strength at 150 mM using saline. Appropriate pH was maintained with phosphate buffer (10 mM, pH 5.5 or 7.4) solutions. DOX-loaded micelle solution was diluted to 1 mg mL^{-1}, and transferred into a dialysis membrane tubing (Spectra/Por, Float-A-Lyzer G2, MWCO = 8–10 kDa). The tubing was immersed in 100 mL of the release medium and kept in a horizontal laboratory shaker maintaining a constant temperature (37 °C) and stirring (100 rpm). Samples were periodically removed and replaced with the same volume of fresh medium. The amount of released DOX was analyzed with a spectrophotometer at 482 nm. The drug release studies were performed in triplicate for each of the samples.

2.11. Dynamic light scattering (DLS)

The hydrodynamic size of the micellar nanoparticles was analyzed using a Brookhaven Instruments BI-200SM system equipped with a 5 mW helium neon laser with a wavelength output of 633 nm. The effective diameter and population distribution were computed from the diffusion coefficient. Measurements were made at 25 °C at an angle of 90°, and each sample was analyzed in triplicate. The micelle solution was filtered using a 0.45 μm membrane filter prior to measurements for all of the experiments.

2.12. Binding affinity of nanoparticles to hydroxyapatite (HA)

The binding affinity of nanoparticles to hydroxyapatite was assessed with free Cy5.5, Cy5.5-loaded nanoparticles or Cy5.5-peptide conjugates.[21] Cy5.5-peptide conjugates were obtained by direct conjugation of Mal-Cy5.5 (Lumiprobe, Russia) with the peptide *via* thiol–maleimide reaction. The samples were dissolved in phosphate buffered saline (pH 7.4) and then subjected to incubation with 1 mg of HA powder (HA, Bio-Gel HTP, DNA grade; BIO-RAD, Hercules, CA) in an eppendorf tube at RT. At predetermined time intervals, the incubation was stopped by centrifugation. The UV absorbance of the supernatant was monitored at a wavelength of 660 nm. Each sample was measured in duplicate.

2.13. Cell culture

Myeloma cells (5TGM1 and ARP-1) and breast cancer cells (MCF-7) were cultured in RPMI1640 containing 10% heat-inactivated fetal calf serum (FCS), 4 mM L-glutamine (Gibco), penicillin (100 U mL^{-1}), and streptomycin (100 μg mL^{-1}) at 37 °C in a humidified atmosphere containing 5% CO_2.

2.14. Cell-proliferation assay

The cells were seeded in 96-well plates at 2000 cells per well in 100 μL of complete medium, and incubated at 37 °C in a 5% CO_2 humidified atmosphere, followed by adding DOX-loaded nanoparticles or blank micelles (25 μL) at pre-determined concentrations. Following 48-hour incubation, 12.5 μL of Presto-Blue™ Cell Viability Reagent (Invitrogen) was added to cultured cells. After incubation for an additional 3 h, the absorbance of the solution was measured at 570 and 600 nm using a microplate reader (Molecular Device). The cell number was calculated according to the manufacturer's instructions, and the cell viability was normalized to that of cells without drug treatment.

2.15. Confocal laser scanning microscopy (CLSM)

Confocal laser scanning microscopy was carried out using an Olympus FV-1000 laser scanning microscope operated with the FLUOVIEW software (Olympus, Tokyo, Japan). Images were produced using the lasers sequentially with a 20× objective lens.

2.16. Biological evaluation of CTSK-pretreated nanoparticles

Cathepsin K (EMD Biosciences) was pre-incubated at 37 °C for 5 min to activate the enzyme in the active site, followed by addition of the nanoparticles. The nanoparticles were incubated with cathepsin K (150 nM) at 37 °C in acetate buffer (0.1 M, pH 5.5). The incubation mixture contained 0.15 μM of cathepsin K, 2.5 mM cysteine, and 5 mM EDTA. After CTSK pretreatment for 30 minutes, nanoparticles were recovered *via* ultrafiltration (MWCO = 100 kDa), and then subjected to zeta potential measurements (Malvern Zetasizer 3000), cell incubation for CLSM observation (Olympus FV-1000) or cytotoxicity evaluations. Nanoparticles were pretreated in the cleavage buffer, but in the absence of CTSK were used as the controls.

2.17. *In vivo* test of nanotherapeutics

The preliminary test of DOX-loaded nanotherapeutics was carried out in a 5TGM1 myeloma cell-induced bone metastatic mouse model. Experiments were approved by the Institutional Animal Care and Use Committee of the University of Utah. To establish the mice with bone manifestations of metastatic

cancers, 1×10^6 5TGM1 cells (in 100 μL PBS) were injected into each mouse through the tail veil and the tumors were allowed to grow for a week. The bone-targeted, CTSK-cleavable nanotherapeutics, as well as the corresponding non-targeted nanotherapeutics (neutral NVs), or free DOX were investigated. The doses of doxorubicin were kept equivalent in different groups. Another group with PBS was used as a negative control. Three C57BL/KaLwRij mice with 5TGM1 inoculations were used for each group. At the time of the experiments, the animal was injected with different therapeutic formulations or controls at a dose of 0.75 mg kg^{-1} twice a week. The tumor burden in the mice was monitored weekly by ELISA measurements of monoclonal immunoglobulin (Ig) in mouse sera. Survival was evaluated from the day of tumor inoculation until death.

2.18. Statistical analysis

All measurements were conducted in duplicate or triplicate and expressed as mean ± standard deviation where indicated. Differences between the mean values were analyzed by two-sided Student's *t* test or one-way ANOVA. The Kaplan–Meier curve and log rank test were used for mouse survival. *P* values of <0.05 are considered statistically significant.

3. Results and discussion

A peptide-conjugated diblock copolymer consisting of a peptide, poly(ethylene glycol) and poly(trimethylene carbonate) (Pep-*b*-PEG-*b*-PTMC) has been synthesized for the first time. PEG was used as the hydrophilic block because of its established role to help NVs escape from protein opsonization and macrophage uptake in the reticuloendothelial system. The rationale behind the choice of PTMC as the hydrophobic block was that PTMC can degrade with a relatively slower rate and have a weak inflammatory effect of degradation compounds, which is a marked advantage over polyesters and particularly attractive to sustained drug delivery application.[22]

The synthesis of a peptide-conjugated diblock copolymer of Pep-*b*-PEG-*b*-PTMC was based on the efficient click reaction between the cysteine terminated Pep peptide and the maleimidevinyl terminated Mal-PEG-*b*-PTMC diblock copolymer, as illustrated in Fig. 1. *Via* the well-established organocatalytic (*i.e.* TU) ring-opening polymerization approach, a non-functional MPEG-*b*-PTMC copolymer could be readily prepared with a defined molecular weight and narrow molecular distribution when using MPEG-OH (M_w = 5000 Da) as the macroinitiator.[23] This strategy was problematic, however, when it came to the synthesis of the maleimide-terminated copolymer of Mal-PEG-*b*-PTMC starting from Mal-PEG-OH. ^{1}H NMR analysis revealed that the maleimidevinylic protons at σ = 6.74 ppm in the product disappeared. Apparently, the maleimide group might be very labile to super basic conditions, and failed to remain intact during the polymerization process. Alternatively, the Mal-PEG_{110}-*b*-$PTMC_{52}$, in which 52 refers to the repeating units of TMC, was successfully synthesized under mild conditions under $Sn(Oct)_2$ catalysis (Fig. 1A). ^{1}H NMR analysis demonstrated that the maleimidevinylic protons at σ = 6.74 ppm in the product remained available after polymerization (Fig. 2). The copolymer composition and number-averaged molecular weight of Mal-PEG_{110}-*b*-$PTMC_{52}$ were determined from the integral ratio of PTMC protons at σ = 4.21 ppm *versus* that of the PEG proton at σ = 3.64 ppm. For comparison purposes, the peptide-free methoxy-terminated $MPEG_{113}$-*b*-$PTMC_{50}$ was also prepared.

Next, we synthesized the functional peptide with a specially designed sequence of $CKGHPGGPQAsp_8$ based on the solid phase peptide synthesis (SPPS) technique (Fig. 1B). The purity (98%) and molecular weight (calculated: 1800.64, found: 1800.54) of the target peptide were confirmed by high-perform-

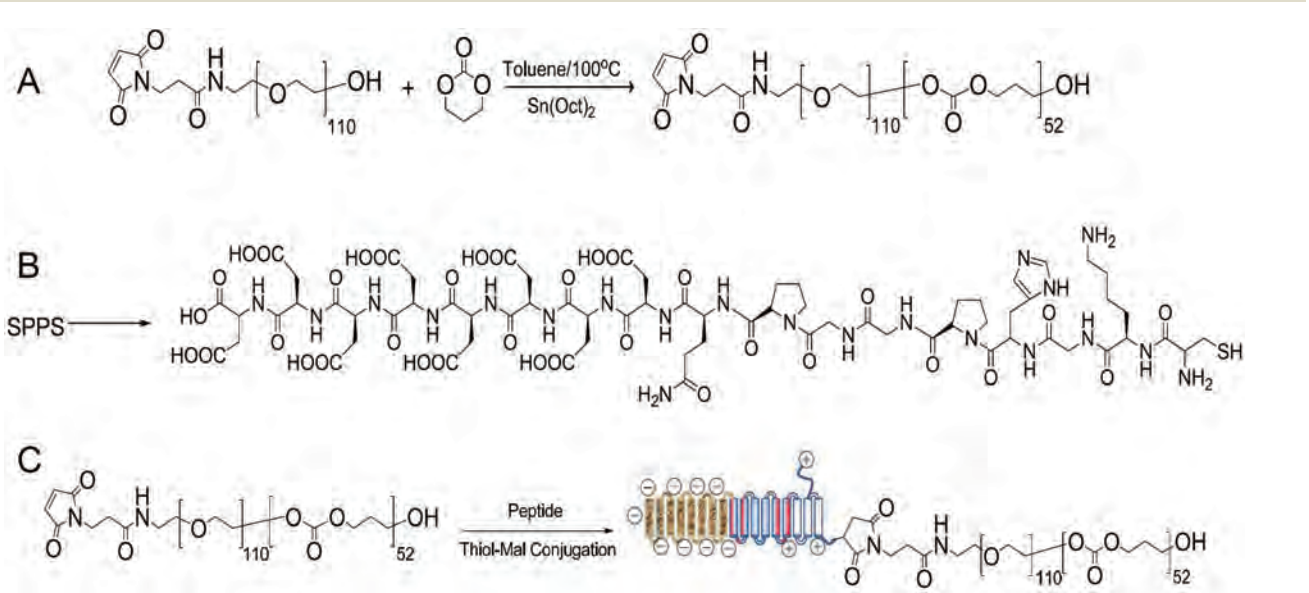

Fig. 1 Synthetic procedure and chemical structure of Mal-PEG_{110}-*b*-$PTMC_{52}$ (A), the Pep peptide (B) and Pep-*b*-PEG_{110}-*b*-$PTMC_{52}$ (C).

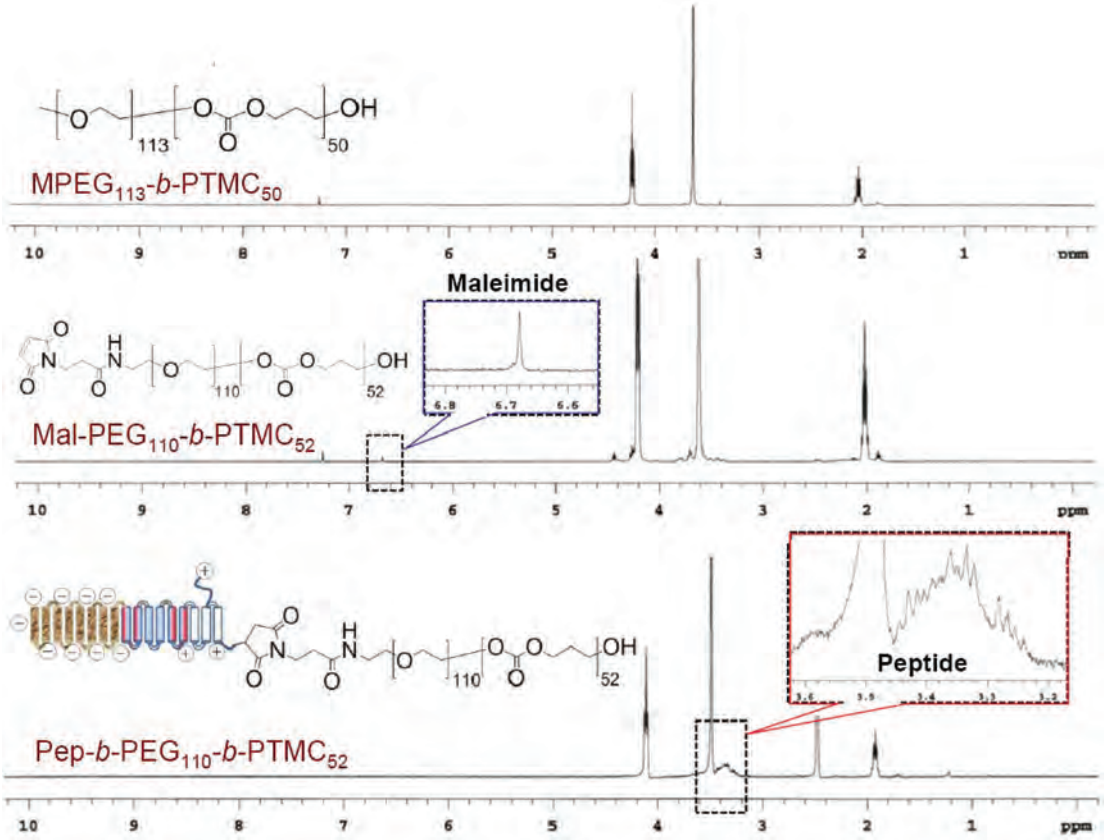

Fig. 2 ^{1}H NMR spectra of $MPEG_{113}$-*b*-$PTMC_{50}$ ($CDCl_3$), Mal-PEG_{110}-*b*-$PTMC_{52}$ ($CDCl_3$) and Pep-*b*-PEG_{110}-*b*-$PTMC_{52}$ (DMSO-d_6).

ance liquid chromatography (HPLC) and matrix-assisted laser desorption/ionization time-of-flight (MALDI-TOF) mass spectrometry, respectively (Fig. S1†). *Via* click chemistry, the chemical conjugation of $CKGHPGGPQAsp_8$ to Mal-PEG_{110}-$PTMC_{52}$ afforded the target copolymer PEP-*b*-PEG_{110}-*b*-$PTMC_{52}$ (Fig. 1C), which was purified by the dialysis method (MWCO = 10 kDa) followed by ultrafiltration treatment. Successful conjugation was verified by ^{1}H NMR, which clearly showed the characteristic resonances of the peptide protons at σ = 3.1–3.6 ppm and complete disappearance of the maleimide-vinylic signal at σ = 6.74 ppm (Fig. 2).

As expected, Pep-*b*-PEG-*b*-PTMC could readily self-assemble into the micelles in aqueous solution like many other amphiphilic copolymers,[24] which was confirmed by the fluorescence assay using pyrene as the probe. According to the excitation spectra of pyrene at different polymer concentrations, the critical micelle concentration (CMC) of Pep-*b*-PEG_{110}-*b*-$PTMC_{52}$ was determined to be approximately 8.02×10^{-3} mg mL^{-1} (Fig. 3C). The mean hydrodynamic diameter of the polymeric micelles was measured by dynamic light scattering (DLS) to be 75 ± 10 nm, showing unimodal size distribution with PDI ~ 0.1.

In principle, the hydrophobic PTMC segments should localize in the inner core of nanomicelles while the peptide and PEG blocks form a corona-type shell due to their highly hydrophilic nature. This core–shell structure was verified by the marked difference between its ^{1}H NMR spectra in DMSO (Fig. 3A) and D_2O (Fig. 3B). All the characteristic signals could be detectable in DMSO-d_6. Unlike this, the proton signals of the PTMC block were significantly suppressed and nearly disappeared in aqueous D_2O but those from hydrophilic blocks remained prominent. Taken together, those characterizations demonstrated that Pep-*b*-PEG_{110}-*b*-$PTMC_{52}$ was able to readily form the NVs with the core–shell architecture in the aqueous medium.

The strong binding ability of Pep-*b*-PEG_{110}-*b*-$PTMC_{52}$ micelles to hydroxyapatite (HA), commonly used as a model mineral to mimic the bone tissue mineral, was examined to preliminarily evaluate the contribution of the peptide functionality to the bone-seeking efficacy.[5–7] A near infra-red fluorescence (NIRF) Cy5.5 probe has been one of the frequently used fluorescence indicators due to its deeper tissue penetration capacity.[25] Cy5.5 was encapsulated into the micellar cores by the dialysis method thus to quantitatively determine the binding affinities of the nanomicelles with and without the peptide functionality.

After incubation for 30 min, approximately 55% of the Pep-*b*-PEG-*b*-PTMC micelles from the solution were rapidly bound to HA. Further incubation for 24 hours led to a moderate increase of HA-binding up to about 66% (Fig. 4). In marked contrast, less than 15% of MPEG-*b*-PTMC micelles or free Cy5.5 were bound to HA across the entire incubation process,

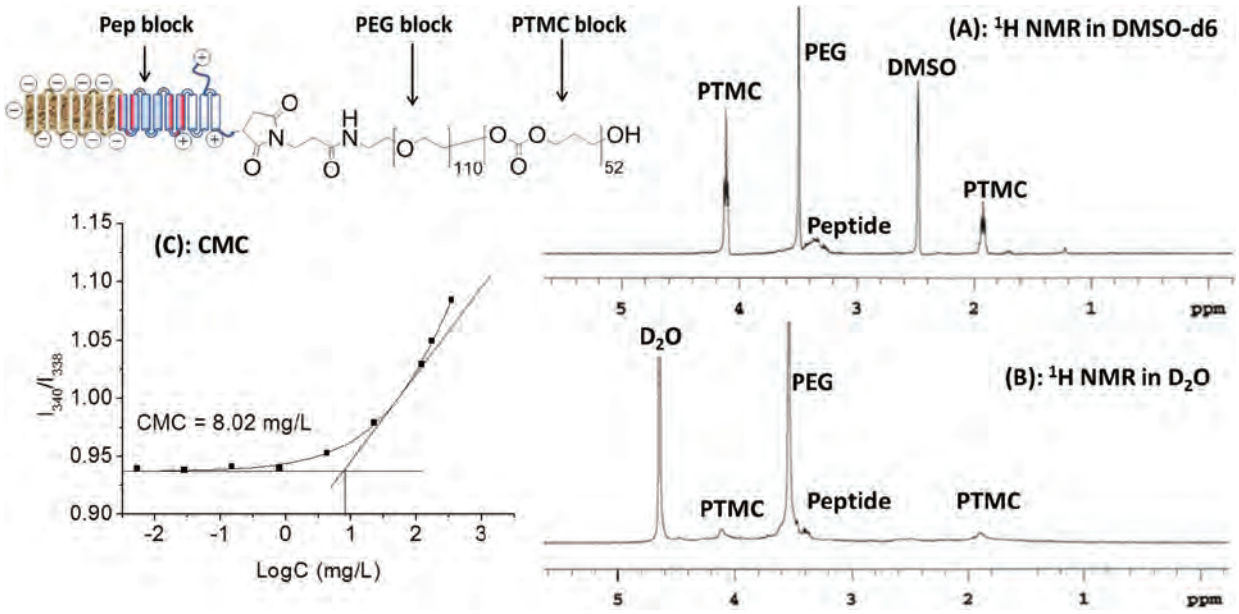

Fig. 3 ^{1}H NMR spectra of Pep-*b*-PEG$_{110}$-*b*-PTMC$_{52}$ in DMSO-d$_6$ (A) and D$_2$O (B); CMC measurement by plotting of the I_{340}/I_{338} ratio against the logarithm of the polymer concentration (C).

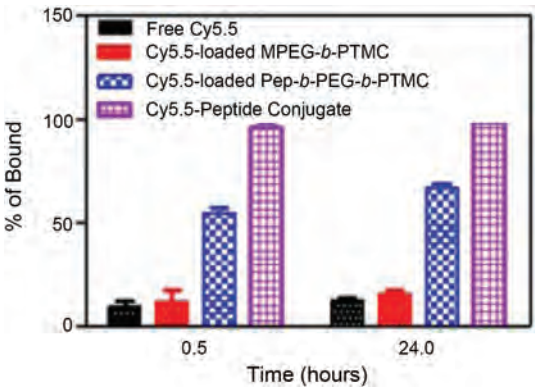

Fig. 4 Binding capacity of various Cy5.5 formulations to the bone mineral HA.

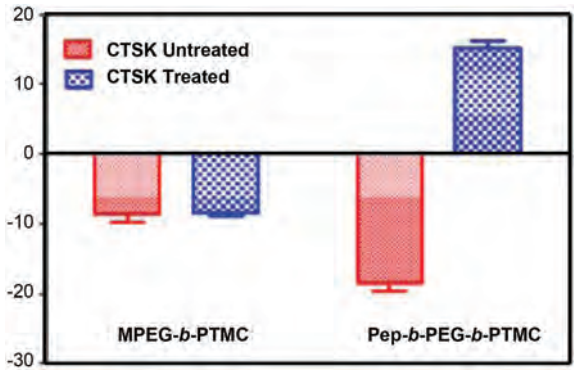

Fig. 5 Change in the zeta potential of Pep-*b*-PEG-*b*-PTMC micelles upon co-incubation with 150 nM CTSK for 30 minutes.

indicating minimal nonspecific binding to HA by the MPEG-*b*-PTMC micelles without the peptide functionality. The low-molecular-weight peptide-Cy5.5 conjugate exhibited a much stronger affinity to HA with complete binding after incubation for 30 min. Those results correlated well with the reported findings that modification with osteotropic Asp$_8$ would dramatically facilitate the specific binding towards HA-rich bone tissue.[26–28] Though the outer PEG shell with steric hindrance may somewhat restrain the complete binding of Pep-*b*-PEG-*b*-PTMC micelles to HA, they still displayed dramatically enhanced HA affinities over Pep-free MPEG-*b*-PTMC micelles after all.

Typically, the decoration of bone-targeting anionic Asp$_8$ to NVs would disfavor the cellular uptake process due to the charge repulsion by the cell membrane, thus impairing the chemotherapy efficacy.[29] Within the structure of Pep-*b*-PEG-*b*-PTMC, a CTSK cleavable substrate (HPGGPQ)[25,30] was specially incorporated to link Asp$_8$ and the rest of the block copolymer. By virtue of such a CTSK-cleavable spacer, it was speculated that the bone metastatic microenvironment featured with CTSK overexpression would induce the enzymatic chain cleavage and the following removal of Asp$_8$ moieties from the shell periphery of the nanomicelles. Of particular interest, this CTSK-induced transition may reverse the surface charge and thus enhance the cellular uptake of the nanomicelles, which was attributed to the remaining cationic peptide residues after Asp$_8$ removal. To verify this speculation, the zeta potentials of polymeric micelles were measured in the presence and absence of CTSK, respectively. Following 30 min treatment with CTSK, the zeta potential of Pep-*b*-PEG-*b*-PTMC micelles had an instantly marked promotion from −18.5 ± 1.9 mV to 15.2 ± 1.8 mV (Fig. 5). Nevertheless, the control experiment without CTSK treatment afforded nearly no variation of the

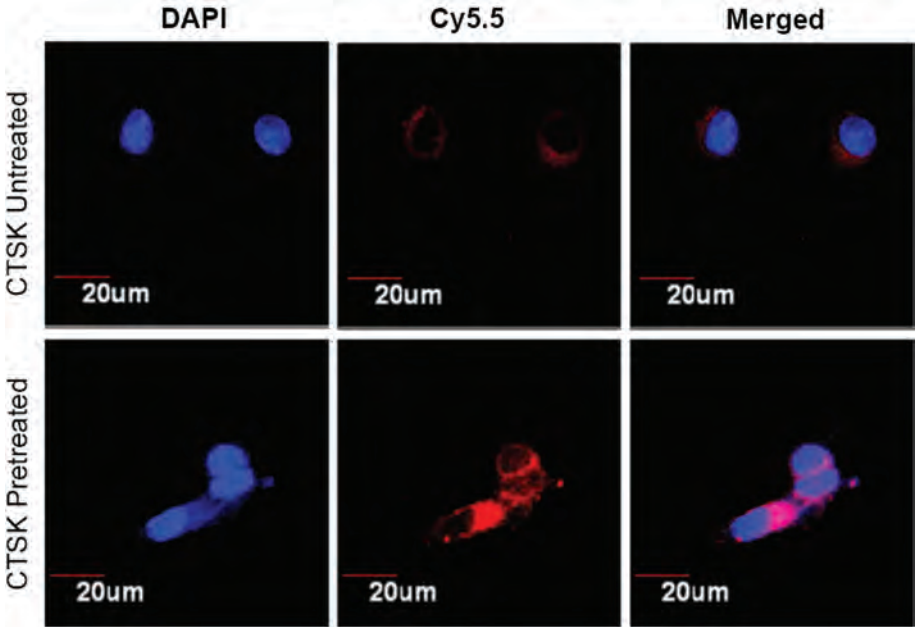

Fig. 6 CLSM images of MCF-7 cells incubated with Pep-*b*-PEG-*b*-PTMC micelles with or without CTSK treatment.

zeta potential. Apparently, it is just CTSK exposure that allowed the charge reversal of the Pep-*b*-PEG-*b*-PTMC micelles.

For comparison, the CTSK-responsiveness of the zeta potential was also tested for MPEG-*b*-PTMC micelles with the identical CTSK treatment. No apparent variation was found upon CTSK exposure and the micellar zeta potential remained almost constant within a narrow range from −8.6 ± 2.1 mV to −8.4 ± 0.7 mV. Those results pointed out that the introduction of the $CKGHPGGPQAsp_8$ functionality indeed played a dominant role in the CTSK-induced negative-to-positive charge conversion of Pep-*b*-PEG-*b*-PTMC micelles.

To evidence the contribution of CTSK-responsive charge reversal to the intracellular internalization, confocal laser scanning microscopy (CLMS) was used to investigate the cellular uptake of polymeric micelles under the conditions with or without CTSK treatment. The nanomicelles assembled from Pep-*b*-PEG-*b*-PTMC were loaded with the Cy5.5 fluorescence indicator, followed by incubation with MCF-7 cells in the presence or absence of CTSK. Following 30 min incubation, the MCF-7 cells were subjected to CLMS observation. As shown in Fig. 6, very weak red fluorescence can be detected in the cells co-incubated with Pep-*b*-PEG-*b*-PTMC micelles in the medium free of CTSK, indicating that few fluorescence-labeled micelles were taken up by MCF-7 cells under this condition. The poor cellular uptake of untreated micelles was reasonably expected, because it was difficult for the negatively charged NVs to be intracellularly internalized owing to the charge repulsion effect. However, upon CTSK exposure, significant fluorescence enhancement was observed from the CLSM images. This was ascribed to the cationic nature of the micelles resulting from CTSK-induced charge-reversal, which was known to favor the approach of NVs to the negatively charged cell membranes and thus facilitate their cellular uptake. For the control of MPEG-*b*-PTMC micelles, it is not strange that a minimal difference was observed between the CLSM images obtained before and after CTSK treatment (data not shown).

The CTSK-dependent cellular uptake of Pep-*b*-PEG-*b*-PTMC nanomicelles seemed very attractive in terms of the chemotherapy potential for bone metastases. It can be noted that those nanomicelles would be hardly taken up by the cells in the normal tissues due to the lack of CTSK expression; once the nanoparticles were guided and accumulated in CTSK-rich environments (*i.e.*, CTSK over-expressed bone metastases lesions), however, the transition to cationic NVs would considerably facilitate the entry into the neighboring tumor cell and thus allow the effective treatment with lower systematical biotoxicity.

To further explore the potential of Pep-*b*-PEG-*b*-PTMC as a drug carrier, an anticancer drug DOX was used as a model drug to investigate the drug loading and release properties. Poorly water-soluble DOX was encapsulated into the micelles of Pep-*b*-PEG-*b*-PTMC or MPEG-*b*-PTMC by the dialysis method. Typical DOX-loading capacity for mPEG-*b*-PTMC micelles was determined as 7.5 ± 0.5% and 22.7 ± 1.5% for DLC (drug loading content) and DLE (drug loading efficiency), respectively. Dramatic increases of DLC (30.0 ± 1%) and DLE (90.1 ± 2%) were observed when Pep-*b*-PEG-*b*-PTMC was used as the drug carrier. Such a high loading efficiency may be the result of the charged nature of Pep-*b*-PEG-*b*-PTMC, for which the outer PEG chains extend more freely and more aggregation numbers per micelle are required to ensure the hydrophilic–hydrophobic balance in the aqueous medium. Thus the DOX drug molecules enter the micelle interior more readily and the larger core is more capable of containing more drug cargos. This is consistent with the finding reported in the literature that charged NVs generally possess high DOX-loading

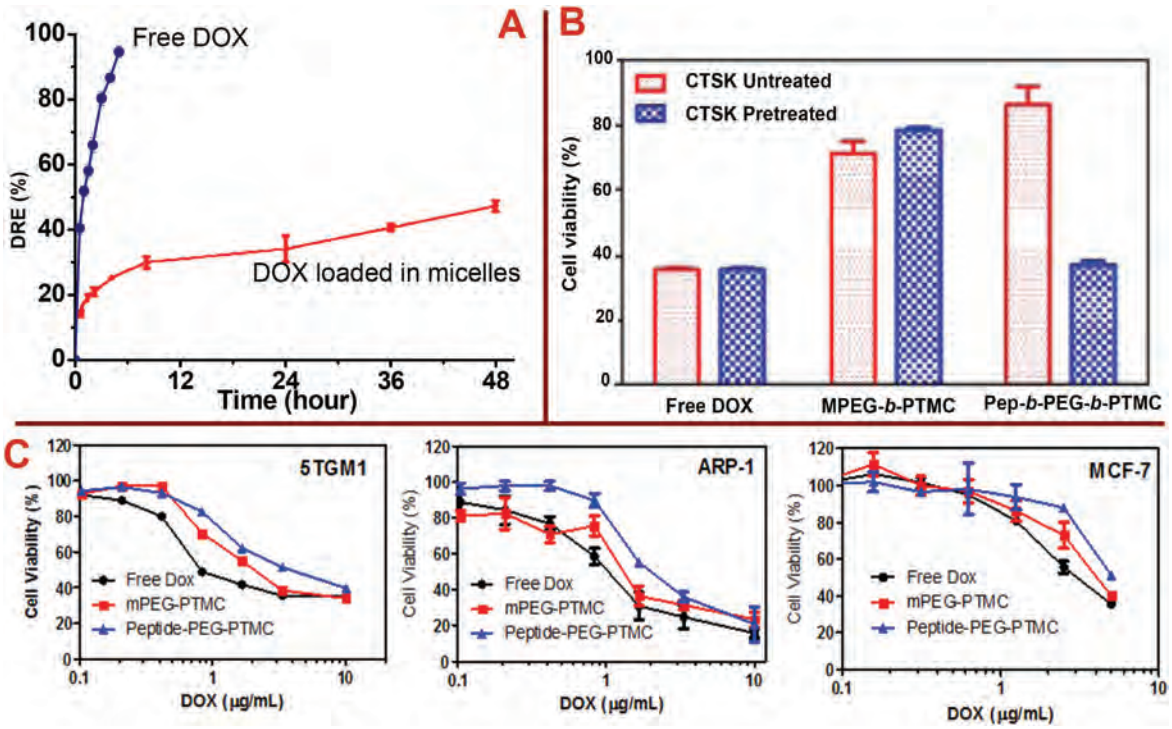

Fig. 7 (A) Cumulative DOX release from the polymeric micelles at pH = 7.4. (B) Cell viability of 5TGM1 cells after incubation with free DOX, DOX-loaded MPEG-*b*-PTMC nanomicelles, and DOX-loaded Pep-*b*-PEG-*b*-PTMC nanomicelles at the same DOX concentration of 1 μg mL^{-1}. Formulations were pre-treated with (blue) or without (red) 150 nM CTSK for 30 minutes. (C) *In vitro* inhibition of 5TGM1, ARP-1 and MCF-7 cells after 48 h incubation with free DOX or DOX-loaded NPs at various doses; data are presented as the average ± standard deviation (n = 3).

capacity.[13,31–33] The representative example is that the highest drug loading (47% w/w) of DOX-loaded micelles reported to date was achieved when anionic polymeric glutamic acid (PGA) was used as a building block within PTMC-*b*-PGA.[31] The *in vitro* drug release study was performed under a simulated physiological condition (pH 7.4). Fig. 7A compares the drug release profiles between the free DOX and the DOX loaded in Pep-*b*-PEG-*b*-PTMC micelles. The results suggested that DOX-loaded micelles exhibited a moderately rapid release in the first stage (around 10%) followed by a sustained release period. The sustained DOX release could be attributed to the hydrophobic interaction of drug molecules with the hydrophobic core of the polymeric micelles.

The *in vitro* cytotoxicity profiles of free DOX or DOX-loaded polymeric micelles were evaluated in the cultured cells including myeloma (the most frequent cancer type for bone metastases) suspension cell lines (5TGM1 and ARP-1) and a breast cancer (the second most frequent cancer type for bone metastases) adherent cell line (MCF-7) by the PrestoBlue™ (Invitrogen) assay. The PrestoBlue assay performed very well to quantitatively measure cell proliferation and to establish the relative viability of both suspension and adherent cells. As shown in Fig. 7C, free DOX exhibited a relatively higher toxic effect than that of both DOX-loaded Pep-free and Pep-functionalized polymeric micelles after 4 h culture. The lowered potency of DOX after encapsulation into the micelles was probably due to the sustained release pattern of DOX from the micelles and delayed drug efficacy in the cultured cells. Overall, DOX-loaded Pep-PEG-*b*-PTMC nanomicelles showed lower cytotoxicity than the Pep-free MPEG-*b*-PTMC micelles. Since the CTSK activity has strong association with the interactions between tumor cells and the bone microenvironment, to give more exact information about the influence of CTSK-responsive charge-reversal on the biological properties of Pep-*b*-PEG-*b*-PTMC micelles, the 5TGM1 cytotoxicity of the DOX-loaded micelles was comparatively explored after a short co-incubation period of 30 min under the conditions with or without CTSK treatment. At an equivalent DOX dose (1 μg mL^{-1}), drug-loaded Pep-*b*-PEG-*b*-PTMC micelles showed lower capability to induce the cell death than the Pep-free MPEG-*b*-PTMC control. CTSK treatment resulted in significant improvement of the drug efficacy in the case of Pep-*b*-PEG-*b*-PTMC micelles (Fig. 7B), which was even comparable to the acute toxicity of free DOX. Noticeably, the CTSK-responsive improvement of toxic effect was not observed for free DOX or DOX-loaded mPEG-*b*-PTMC micelles. This marked contrast manifested a close tie between the CTSK responsiveness and the Pep functionality in the micelles, which contributed much to the enhanced drug efficacy. In combination with the result of intracellular internalization obtained from confocal images, it is naturally inferred that the anionic nature associated with the targeting Asp_8 moieties would disfavor the intracellular internalization of the Pep-*b*-PEG-*b*-PTMC micelles and therefore impair the drug efficacy, whereas CTSK-responsive

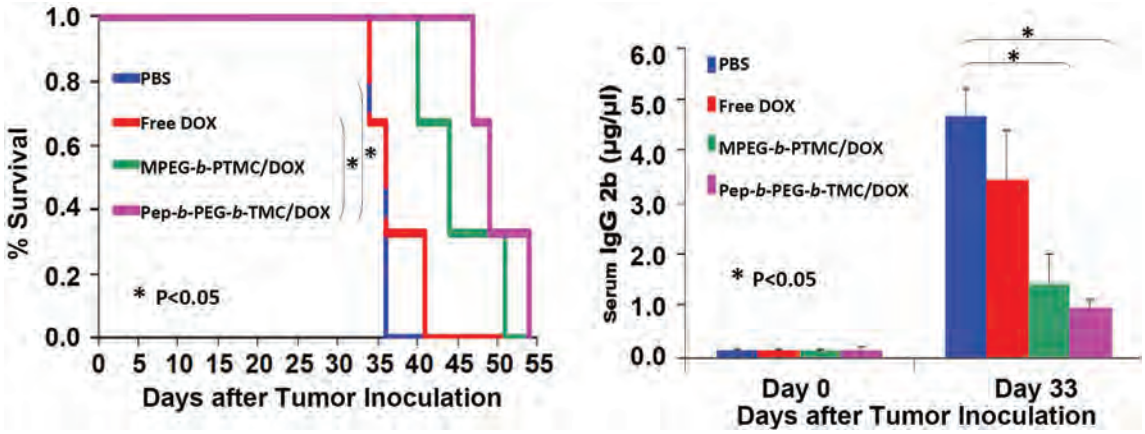

Fig. 8 (A) Efficacy of free DOX or DOX-loaded nanomicelles in bone metastatic 5TGM1 mice bearing myeloma; (B) Kaplan–Meier survival curves of mice following tumor injection and treatments. Relative tumour burden in mice was determined by the IgG 2b level in sera. *$P < 0.05$ ($n = 3$).

charge reversal may more or less overcome this biological barrier.

Despite the advance of drug delivery nanosystems for bone metastases, to the best of our knowledge, nearly no *in vivo* efficacy evaluation in animal studies have yet been reported. This could be in part ascribed to the limited availability of suitable detection means for the disease progression of bone metastases. Herein, a preliminary *in vivo* study was conducted to test the efficacy of DOX-loaded Pep-*b*-PEG-*b*-PTMC nanomicelles in a 5TGM1-induced myeloma-bearing mice model. Multiple myeloma is the most frequent cancer-induced osteolytic disease,[1,2] which intends to invade skeletal tissues in a similar mechanism to cancer cells that interact with the bone marrow microenvironment.[34] Likewise, the interactions between myeloma cells and osteoclasts yield substantial cathepsin K up-regulation, resulting in osteolytic lesions.[35] Noticeably, the real-time tumor burden in 5TGM1 mice can be easily monitored by measuring the 5TGM1 idiotype (IgG2b) in mouse sera.[36] The higher IgG2b level in sera, the bigger tumor in the body. This is a distinct advantage since the progression of other types of cancers can only be identified with advanced imaging modalities (μCT, X-ray, *etc.*).[37] Myeloma-bearing 5TGM1 mice were established through inoculation of 5TGM1 cells (1×10^6 cells in 100 μL PBS) *via* tail veil injection, and the tumors were allowed to develop and grow for one week before initiating study treatments. The mice were injected twice weekly with different therapeutic formulations at an equivalent DOX dose (0.75 mg kg^{-1}) or blank PBS, and the IgG2b level in sera was monitored by ELISA measurements.

As shown in Fig. 8A, the myeloma-bearing 5TGM1 mice group treated with DOX-loaded Pep-*b*-PEG-*b*-PTMC micelles showed prolonged survival rate in comparison with the control groups with the administration of DOX-loaded MPEG-*b*-PTMC micelles, free DOX or blank PBS. Since the tumor burden was positively correlated with the IgG2b level, the data in Fig. 8B distinctly indicated that Pep-*b*-PEG-*b*-PTMC/DOX nanotherapeutic was meanwhile more effective to slow down tumor growth than the other formulations with the equivalent DOX dose. Together with the *in vitro* results, the observed improvement of both *in vivo* systematic biosafety and drug efficacy manifested the superiority of our pathology-specific design by combining both the advantages of efficient DOX delivery to bone metastatic tissues and CTSK-responsive cellular uptake of DOX within lesion sites.

4. Conclusions

Cancer induced bone metastases often lead to substantial morbidity and mortality, which remain a significant therapeutic challenge for cancer treatment. In attempts to address this challenge, a peptide decoration strategy was proposed to render the NVs both the bone-seeking function and the charge-reversal capability in response to the pathological microenvironment. The nanomicelles self-assembled from the Pep-*b*-PEG-*b*-PTMC polymer showed strong apatite binding affinity and readily underwent the negative-to-positive charge reversal upon exposure to CTSK, an overexpressed enzyme in bone metastatic microenvironments. This unique characteristic led to dramatically enhanced cellular uptake within bone metastatic sites in a pathology-responsive manner, thus improving the drug efficacy of the loaded DOX *in vitro* and *in vivo*. Although our attempt presented herein for the enhanced bone metastasis chemotherapy is still in an initial stage, the obtained *in vivo* and *in intro* results are fairly encouraging. More attractively, the success of this strategy may open a new avenue to chemotherapy for the malignant diseases in bone tissue, including but not limited to bone metastases, provided that the development of therapy for those diseases involves overexpression of certain enzymes.

Acknowledgements

This research was supported by NIH (R01CA166941, X. Wang), the Department of Defense (W81XWH1110307 and

W81XWH1310240, X. Wang), the University of Utah CCTS Pilot Award (U59004183, X. Wang) from the NIH National Center for Research Resources (UL1RR025746), the TRP Award (6246-11, F. Zhan) from the Leukemia & Lymphoma Society, and the National Natural Science Foundation of China (grant no. 21374085, J. Feng).

Notes and references

1 G. D. Roodman, *N Engl. J. Med.*, 2004, **350**(16), 1655–1664.
2 L. S. Loftus, S. Edwards-Bennett and G. H. Sokol, *Cancer Control*, 2012, **19**(2), 145–153.
3 C. M. Bagi, *Adv. Drug Delivery Rev.*, 2005, **57**(7), 995–1010.
4 R. E. Coleman, *Nat. Rev. Clin. Oncol.*, 2012, **9**(2), 76–78.
5 D. Wang, S. C. Miller, P. Kopeckova and J. Kopecek, *Adv. Drug Delivery Rev.*, 2005, **57**(7), 1049–1076.
6 K. Miller, R. Erez, E. Segal, D. Shabat and R. Satchi-Fainaro, *Angew. Chem., Int. Ed.*, 2009, **48**(16), 2949–2954.
7 D. Wang, S. C. Miller, L. S. Shlyakhtenko, A. M. Portillo, X. M. Liu, K. Papangkorn, P. Kopekova, Y. Lyubchenko, W. I. Higuchi and J. Kopecek, *Bioconjugate Chem.*, 2007, **18**(5), 1375–1378.
8 Q. Zhao, Y. Jia and Y. Xiao, *Biochem. Biophys. Res. Commun.*, 2009, **380**(4), 721–723.
9 C. Le Gall, A. Bellahcene, E. Bonnelye, J. A. Gasser, V. Castronovo, J. Green, J. Zimmermann and P. Clezardin, *Cancer Res.*, 2007, **67**(20), 9894–9902.
10 R. N. Pearse, *Clin. Breast Cancer*, 2007, **8**, S35–S45.
11 C. Le Gall, E. Bonnelye and P. Clezardin, *Curr. Opin. Support. Palliat. Care*, 2008, **2**(3), 218–222.
12 J. Sturge, M. P. Caley and J. Waxman, *Nat. Rev. Clin. Oncol.*, 2011, **8**(6), 357–368.
13 J. Z. Du, T. M. Sun, W. J. Song, J. Wu and J. Wang, *Angew. Chem., Int. Ed.*, 2010, **49**(21), 3621–3626.
14 Y. Lee, T. Ishii, H. Cabral, H. J. Kim, J. H. Seo, N. Nishiyama, H. Oshima, K. Osada and K. Kataoka, *Angew. Chem., Int. Ed.*, 2009, **48**(29), 5309–5312.
15 Y. Lee, K. Miyata, M. Oba, T. Ishii, S. Fukushima, M. Han, H. Koyama, N. Nishiyama and K. Kataoka, *Angew. Chem., Int. Ed.*, 2008, **47**(28), 5163–5166.
16 P. S. Xu, E. A. Van Kirk, Y. H. Zhan, W. J. Murdoch, M. Radosz and Y. Q. Shen, *Angew. Chem., Int. Ed.*, 2007, **46**(26), 4999–5002.
17 T. Ariga, T. Takata and T. Endo, *Macromolecules*, 1997, **30**(4), 737–744.
18 A. P. Dove, R. C. Pratt, B. G. Lohmeijer, R. M. Waymouth and J. L. Hedrick, *J. Am. Chem. Soc.*, 2005, **127**(40), 13798–13799.
19 H. R. Kricheldorf, I. Kreiser-Saunders and A. Stricker, *Macromolecules*, 2000, **33**(3), 702–709.
20 J. Z. Du, D. P. Chen, Y. C. Wang, C. S. Xiao, Y. J. Lu, J. Wang and G. Z. Zhang, *Biomacromolecules*, 2006, **7**(6), 1898–1903.
21 H. Z. Pan, P. Kopeckova, D. Wang, J. Y. Yang, S. Miller and J. Kopecek, *J. Drug Target*, 2006, **14**(6), 425–435.
22 J. Feng, X. Z. Zhang and R. X. Zhuo, *Prog. Polym. Sci.*, 2012, **37**(2), 211–236.
23 F. Nederberg, B. G. G. Lohmeijer, F. Leibfarth, R. C. Pratt, J. Choi, A. P. Dove, R. M. Waymouth and J. L. Hedrick, *Biomacromolecules*, 2007, **8**(1), 153–160.
24 L. Liu, K. Xu, H. Wang, P. K. Tan, W. Fan, S. S. Venkatraman, L. Li and Y. Y. Yang, *Nat. Nanotechnol.*, 2009, **4**(7), 457–463.
25 K. M. Kozloff, L. Quinti, S. Patntirapong, P. V. Hauschka, C. H. Tung, R. Weissleder and U. Mahmood, *Bone*, 2009, **44**(2), 190–198.
26 M. B. Murphy, J. D. Hartgerink, A. Goepferich and A. G. Mikos, *Biomacromolecules*, 2007, **8**(7), 2237–2243.
27 S. Kasugai, R. Fujisawa, Y. Waki, K. Miyamoto and K. Ohya, *J. Bone Miner. Res.*, 2000, **15**(5), 936–943.
28 D. Wang, S. Miller, M. Sima, P. Kopekova and J. Kopecek, *Bioconjugate Chem.*, 2003, **14**(5), 853–859.
29 K. Xiao, Y. Li, J. Luo, J. S. Lee, W. Xiao, A. M. Gonik, R. G. Agarwal and K. S. Lam, *Biomaterials*, 2011, **32**(13), 3435–3446.
30 F. A. Jaffer, D. E. Kim, L. Quinti, C. H. Tung, E. Aikawa, A. N. Pande, R. H. Kohler, G. P. Shi, P. Libby and R. Weissleder, *Circulation*, 2007, **115**(17), 2292–2298.
31 C. Sanson, C. Schatz, J. F. Le Meins, A. Soum, J. Thevenot, E. Garanger and S. Lecommandoux, *J. Controlled Release*, 2010, **147**(3), 428–435.
32 C. Yang, J. Tan, W. Cheng, A. Attia, C. Tan, Y. Ting, A. Nelson, J. L. Hedrick and Y. Y. Yang, *Nano Today*, 2009, **5**, 515–523.
33 N. Wiradharma, Y. Zhang, S. Venkataraman, J. L. Hedrick and Y. Y. Yang, *Nano Today*, 2009, **4**(4), 302–317.
34 J. A. Fowler, C. M. Edwards and P. I. Croucher, *Bone*, 2011, **48**(1), 121–128.
35 M. Hecht, I. von Metzler, K. Sack, M. Kaiser and O. Sezer, *Exp. Cell Res.*, 2008, **314**(5), 1082–1093.
36 B. O. Oyajobi, G. Franchin, P. J. Williams, D. Pulkrabek, A. Gupta, S. Munoz, B. Grubbs, M. Zhao, D. Chen, B. Sherry and G. R. Mundy, *Blood*, 2003, **102**(1), 311–319.
37 T. J. Rosol, S. H. Tannehill-Gregg, B. E. LeRoy, S. Mandl and C. H. Contag, *Cancer*, 2003, **97**(3), 748–757.

IMPaCT

Innovative Minds in Prostate Cancer Today

Young Investigators Meeting


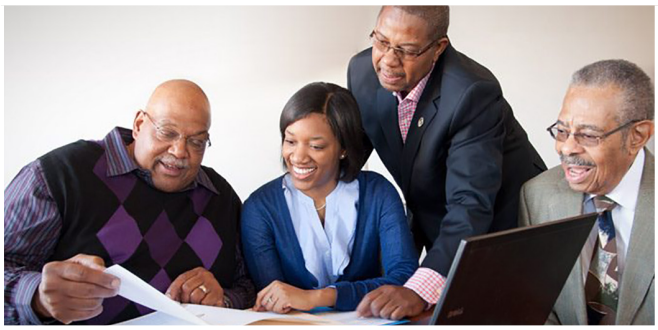
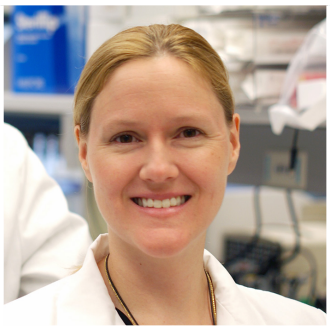

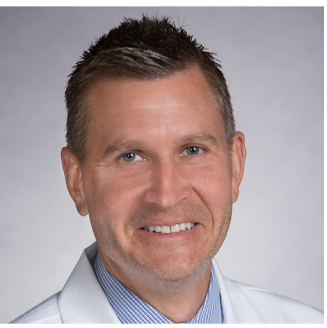
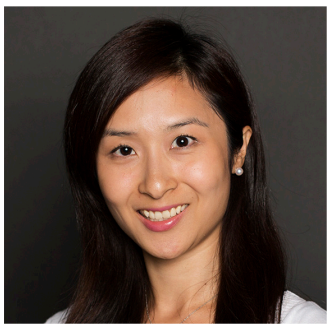
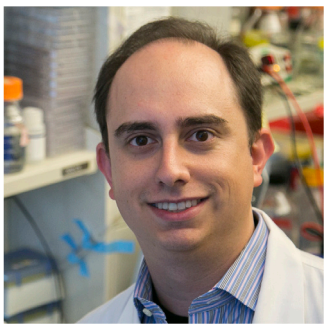

August 4-5, 2016
Baltimore, Maryland

PROCEEDINGS

Table of Contents

Table of Contents (cont.)

Table of Contents (cont.)

Design and Development of Prostate Cancer-Responsive Nanotherapeutics

X Wang, L Zhan, T Liu, and G Colvin

University of Utah

Background: Advanced prostate cancer frequently leads to skeletal complications that are very difficult to treat and result in pain, bone fractures, nerve compression, morbidity, and often mortality, and it is considered to be an incurable disease. Our research has addressed such a challenge by innovative design of bio-responsive and prostate-specific drug delivery systems. Our research strategy is based on recent advances in the development and optimization of prostate-specific antigen (PSA) that have provided more specific ligands to prostate cancer. The major objective from our research is to develop effective therapeutic approaches that are favourably responsive to prostate cancer-induced microenvironment, thus improving prostate cancer therapy.

Methods: Three approaches in order to improve specificity and responsiveness of nanotherapeutics to prostate cancer have been designed. The first one is to take advantage of a prostate-specific membrane antigen (PSMA) with high affinity (K_i = 8 nm), namely 2-[3-(1,3-dicarboxypropyl)ureido]pentanedioic acid (DUPA). The second approach is to utilize a PSA-cleavable peptide, specifically Arg-Ser-Ser-Tyr-Tyr-Ser-Leu-Lys, as a linker for selectively releasing an anticancer agent (docetaxel, DTX) from nanotherapeutics. The third approach is to explore a charge reversal strategy by using a substrate possessing both features of PSA-specificity and bone-targeting capacity. The chemical and biophysical properties of nanotherapeutics, including chemical structure and composition, size, surface charge, drug loading capacity, drug release profile, and binding affinity to hydroxylapatite, have been determined. The nanotherapeutics have further been investigated in terms of cellular uptake and cytotoxicity in cultured prostate cells. Evaluation of nanotherapeutics for biodistribution and antitumor efficacy in animals is ongoing.

Results: The designed biomaterials have been successfully synthesized. DTX has been loaded into biopolymers via a chemical conjugation strategy with approximately 10% drug loading content in polymers. Their molecular structures have been confirmed by nuclear magnetic resonance. The obtained biomaterials are able to spontaneously form nanosized constructs with the size of approximately 100 nm. DUPA-modified block polymer has shown moderate improvement over controls in terms of cellular uptake by a PSA-expressing prostate cancer cell line (LNCaP). Interestingly, Arg-Ser-Ser-Tyr-Tyr-Ser-Leu-Lys modified biopolymer has shown selective and effective drug release in LNCaP cells. More importantly, after functionalization with a substrate containing both polyaspartic acid and PSA-cleavable peptide, nanotherapeutics not only exhibit rapid hydroxyl apatite binding capacity, but also demonstrate surface charge reversal profile, indicating their potential application for prostate cancer-induced bone metastasis.

Conclusions: The combination of bone-targeting moiety and PSA-cleavable linker in nanotherapeutics is a feasible and promising strategy to improve their bioavailability, skeleton-selectivity, and PSA-specificity for prostate cancer therapy.

Impact Statement: The encouraging results from this study may prompt the development of bone-targeted, enzyme-triggered drug delivery systems to improve their affinity to skeletal tissue, enhance selectivity for prostate cancer, and improve efficacy of anti-cancer agents, thus facilitating development of therapeutic strategy for prostate cancer.